Check for updates

Cellulose nanomaterial metrology: microscopy measurements†

Linda J. Johnston [ID]

Cellulose nanomaterials are increasingly used for a wide variety of applications. Adequate characterization of these materials is required for quality control during production, to distinguish between materials synthesized by different methods, by different suppliers or from difference cellulose biomass sources, to facilitate development of applications and for regulatory purposes. Here we review recent microscopy measurements for the three main types of cellulose nanomaterials: cellulose nanocrystals, individual cellulose nanofibrils and cellulose nanofibrils. Atomic force microscopy and both scanning and transmission electron microscopy are covered with a focus on recent studies that have metrological rigor, rather than qualitative investigations. In some cases results are compared to those obtained by other methods that are more likely to see widespread use for routine quality control measurements. Detailed studies that use microscopy to provide insight on fundamental material properties (*e.g.*, chiral properties) are also included. Particle size and morphology are important properties but are challenging to measure for cellulose nanomaterials due to the rod or fibril shaped particles, their propensity to agglomerate and aggregate, their low contrast for electron microscopy and, for cellulose nanofibrils, the complex branched and interconnected structures. Overall, the results show that there are now a number of studies in which attention to metrological detail has resulted in measurements that allow one to compare and distinguish between different materials, although there are still examples for which it is not possible to draw conclusions on size differences. The use of detailed microscopy protocols that yield accurate and reliable results will be beneficial in material production and addressing regulatory requirements and will allow the validation of other methods that are more amenable to routine measurements.

Introduction

Cellulose nanomaterials (CNMs) have attracted considerable attention recently since they are generated from cellulose, the world's most abundant biopolymer, making them a sustainable replacement for petroleum-based products that are currently in widespread usage. They are widely available materials that are renewable and sustainable and have a range of impressive and useful properties. These include their high aspect ratio, high crystallinity, mechanical strength, thermal stability, ease of surface functionalization, anticipated lack of toxicity and self-assembly properties. As a result, they are now being used or developed for a diverse range of applications including adhesives, inks, drilling fluids, filtration, paper products, textiles, optical films, polymer composites, electronic components, automotive sector, food coatings, cosmetics, tissue engineering scaffolds and drug delivery.[1–9]

Cellulose nanomaterials are defined as materials composed predominantly of cellulose with any external dimension in the nanoscale or materials with internal or surface structure in the nanoscale and composed predominantly of cellulose; there are three main categories of CNMs.[10] Cellulose nanocrystals (CNCs) are composed predominantly of cellulose with crystalline and paracrystalline regions and have at least one elementary fibril and no longitudinal splits. Note that an elementary fibril is biosynthesized by a single terminal enzyme complex and has a configuration of cellulose chains specific to the cellulose-producing species The typical aspect ratio of CNCs is between 5 and 50 and they do not exhibit interparticle entanglement or network-like structures. They are generated by acid hydrolysis of wood pulp or other cellulose biomass sources, which typically leads to negatively charged surface groups such as sulfate half esters or phosphates.[11]

Individual cellulose nanofibrils (iCNFs) are discrete cellulose nanofibrils composed of at least one elementary fibril with ionic groups on the surface.[12] They are typically generated by TEMPO (2,2,6,6-tetramethylpiperidine-1-oxyl radical)-

Metrology Research Center, National Research Council Canada, Ottawa, ON, Canada K1A 0R6. E-mail: Linda.Johnston@nrc-cnrc.gc.ca

mediated oxidation coupled with mild mechanical disintegration in water, leading to carboxylic acid groups on their surface.[13] A number of other routes that introduce a significant number of charged surface groups can also be used.[5] Cellulose nanofibrils (CNFs) are nanofibers composed of at least one elementary fibril that contain branches, a significant fraction of which are on the nanoscale. Dimensions are typically 3 to 100 nm in cross section and up to 100 μm in length. Cellulose nanofibrils form entanglements between particles or network-like structures, may contain hemicellulose and or lignin if formed from plant sources and may have functional groups on their surface. Their formation employs mechanical treatment of pulps using homogenizers, mechanical refiners, microfluidizers or grinding equipment.[2] Representative images of the three types of CNMs are shown in Fig. 1. Other cellulose based materials such as microfibrillated cellulose may have a (small) nano component[14] but are outside the scope of the current review.

Many CNM applications require an in-depth understanding of the material properties and how they impact performance. Despite the importance of the physical chemical properties, there are relatively few validated protocols that allow for reproducible characterization of the materials. This is in contrast to the available standards for measurements of non-nano cellulose-based materials (ISO TC 6 Pulp Paper & Boards) and inorganic nanomaterials (ISO TC 229 Nanotechnologies; silica, metal and metal oxide nanoparticles, quantum dots). Size (length, cross section), aspect ratio and morphology (shape, branching) as well as surface chemistry and crystallinity are important parameters to assess. This helps to define and distinguish between different materials and impacts on properties that are important for applications.

Adequate characterization of CNMs is also important for determining their classification as a nanomaterial and obtaining regulatory approval for their use. One driving force for a better understanding of the dimensional properties of CNMs is the recently revised European definition of a nanomaterial.[18] The revised definition states that a nanomaterial is a natural, incidental or manufactured material consisting of solid particles that are present, either on their own or as identifiable constituent particles in aggregates or agglomerates, and where 50% or more of the particles in the number-based size distribution fall within the 1 nm–100 nm range or meet similar criteria for rod or plate-shaped materials. This new definition is meant to be included in legislation for various European Union agencies and to facilitate a streamlined approach to dealing with nanomaterials in different sectors. However, the regulatory definition varies with the jurisdiction, and in some cases has a mass-based rather than a number-based criterion, as summarized in recent reviews.[19,20] For example, the nano-specific guidance of the US Toxics Substance Control Act applies to chemical substances that are "solids at 25 °C and standard atmospheric pressure, manufactured or processed in a form where any particles, including aggregates and agglomerates, are in the size range of 1–100 nm in at least one dimension and are manufactured or processed to exhibit one or more unique and novel properties".[21] Materials with less than 1% by weight of any particles, including aggregates and agglomerates, between 1 to 100 nm are excluded. In Canada, the working definition has a similar size range and statement on novel properties, but includes both mass and number-based criteria with thresholds of 1% and 10%, respectively.[22]

This review will focus on investigations of CNM size and morphology with an emphasis on a critical review of studies that are aimed at metrologically rigorous measurements, rather than the use of imaging methods for a qualitative assessment of size and shape. Although qualitative measurements are frequently used during preparation and characterization of materials, they do not allow one to distinguish between materials, either within a single lab using similar instrumentation and methods, or between laboratories. Qualitative measurements of a small number of particles with no assessment of measurement uncertainty also fail to provide sufficient information to allow comparison of materials from different cellulose sources. The following statement paraphrased from a recent review of CNM characterization accurately describes the need for metrologically relevant methods and data. "Key to the advancement of these applications will be the development of measurement protocols necessary for consistent, reliable and accurate characterization of CNMs that
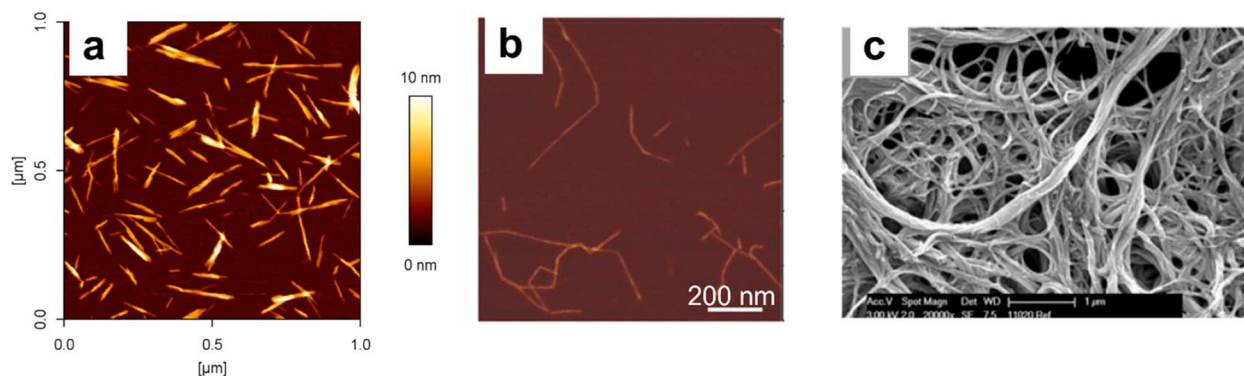

Fig. 1 Images of the three main types of CNMs: (a) CNCs, AFM, (b) iCNFs, AFM, (c) CNFs, SEM. This figure has been adapted from references[15] (a),[16] (b),[17] (c) with permission from Springer Nature, copyright 2018, Wiley, copyright 2016 and De Gruyter, copyright 2014.

are critical for expanding the mechanistic understanding of the various processes needed for optimizing CNM utilization. More consistent protocols and measurements will help reduce systematic uncertainty in data measurements, allowing higher confidence when comparing results between research groups. It has become essential to be able to describe CNMs consistently without confusion, whether it is for scientific curiosity, quality control, product development or selling to different markets".[23] This review will cover primarily transmission electron microscopy (TEM), scanning electron microscopy (SEM) and atomic force microscopy (AFM), all of which have been widely used. However, in some cases, comparisons with more readily accessible methods that are useful for quality control of material properties will also be discussed; these include light scattering methods, optical imaging, small angle X-ray scattering (SAXS) and rheology. Use of microscopy methods to obtain information on fundamental mechanisms of behavior of these materials is also included. The focus is primarily on recent studies (since approximately 2016) that have measured particle size distributions for a sufficient number of particles to ensure metrological validity and investigations of nanoscale structure that provide fundamental insight on the properties and behavior of CNCs.

The three types of CNM each present additional challenges when compared to simple inorganic nanomaterials which frequently have approximately spherical shapes, relatively narrow size distributions and for which aggregation and agglomeration can often be minimized.[24–26] The level of difficulty is lowest for CNCs, for which length and width can typically be assessed in the same image set and for which it is possible to control the extent of particle agglomeration and aggregation. However, the irregular rod shape of the CNCs does present some challenges in deciding exactly how the cross section should be measured. iCNFs are similar to CNCs; measurement of their cross section is more straightforward since they are typically comprised of a single elementary fibril, and can be deposited on a substrate for imaging with relatively modest agglomeration. However, they have the added complexity of having kinked structures and often have higher aspect ratios than CNCs, which makes assessment of length somewhat more challenging. The challenges of assessing dimensional parameters for typical CNFs which have highly branched and interconnected structures is considerably higher. A number of studies have only measured particle width but the complex tree-like structure makes it challenging to decide how the branch width measurements should be done and whether a representative data set has been obtained.

Cellulose nanocrystals

Cellulose nanocrystals are straight rod or spindle-shaped particles, as noted above, and are the most straightforward CNM type for detailed examination of their size and morphology. As such there have been quite a large number of studies that have used AFM and TEM (and occasionally SEM) to investigate their

size. Most early studies have been summarized in recent reviews[2,27] and indicate that CNCs from wood pulps have mean cross sectional dimensions of 3–8 nm with mean lengths in the range of 50 nm up to several hundred nm. By contrast tunicate-derived CNCs have much higher aspect ratios with rectangular cross sections (mean values of 8 nm and 20 nm) and lengths up to several μm and bacteria-derived CNCs are also larger with reported AFM mean heights of 14 nm and lengths of 1.1 μm. Images of longer CNCs such as those from tunicate or bacterial sources have some particles that have slight curvature along their long axis.[28,29]

The variation in CNM morphology is related to the biosynthesis of cellulose, a linear polymer of D-glucose units, by a terminal enzyme complex.[2,8,30] Individual cellulose chains are produced in parallel by the enzyme complex and assemble into elementary fibrils with individual polymer chains held together by van der Waals forces and hydrogen bonding. Different plants and organisms have terminal enzyme complexes that assemble different numbers of individual polymer chains to give the elementary fibril, resulting in fibrils that vary in their cross-sectional dimensions. The elementary fibrils are then assembled in a hierarchical fashion to give larger microfibrils and ultimately fibers that contain other components such as lignin and pectin and provide the structural integrity of plants.[2,8] The processing conditions that are used to liberate CNMs from the pre-processed cellulose biomass also impact the particle morphology. There is an extensive body of literature that examines the properties of CNCs generated from different cellulose biomass sources, particularly from plants, and explores the effect of changes in the acid hydrolysis conditions on the material properties, including CNC yield, degree of polymerization, size, crystallinity and surface charge. A summary of this work will not be presented here but the interested reader can find information in several comprehensive reviews.[4,6,7,11,31,32]

Sample preparation for AFM

Sample preparation is a key factor for microscopy measurements and one aims to ensure samples have adequately dispersed material that minimizes the extent of agglomerated particles but maximizes the number of analyzable particles/image. Given the propensity of CNCs to agglomerate and/or aggregate, preparation of the initial suspension should be done with care. Probe sonication has typically been used to disperse CNCs, particularly when the sample is sourced as a dry powder that requires redispersion for characterization or for development of applications. In a number of studies dynamic light scattering (DLS), rheology or TEM has been used to assess the sonication efficiency and select an energy that minimizes agglomerates/aggregates without damaging the CNCs.[15,33–38] Although neither DLS nor rheology provides direct information on the number of remaining agglomerates, both have been shown to be useful for obtaining a repeatable CNC dispersion.[15,35,39] A recent study has compared results for five methods for monitoring sample dispersion in order to assess their suitability for determining an optimal sonication

level for commercial CNCs.[40] The methods included rheology, AFM, DLS, interferometric scattering microscopy and cluster-triggered emission autofluorescence spectroscopy. The AFM images of samples prepared with different sonication energies were analyzed in detail to estimate particle volume and agglomerate fraction, as well as height, significantly increasing the information content that is generally obtained from this method. Overall, the results indicated that AFM height, rheology and the two microscopy/spectroscopy methods were sufficiently sensitive to the transition from agglomerates to individual CNCs and gave similar results (Fig. 2). By contrast DLS and AFM volume and agglomerate fraction continued to show apparent changes in dispersion level for higher total sonication energies, leading to the possibility that some CNC degradation will occur if these methods are used to monitor samples. The authors noted that the formation of agglomerates during sample deposition on the AFM substrate will limit the utility of monitoring agglomerate fraction. The image resolution used and the assumptions used to calculate volume may also contribute. In any case, alternatives to AFM for routine monitoring of dispersion are certainly necessary since the time commitment required to assess AFM height is a significant disadvantage for routine measurements.

Deposition of CNCs for AFM has generally used either mica or silicon wafers as the support and a large number of studies have coated the surface with a cationic polymer layer (typically poly-L-lysine, PLL, or poly(allylamine hydrochloride), PAH) or treated the surface with (3-aminopropyl)triethoxysilane (APTES) to minimize agglomeration and better immobilize particles. Almost all studies which have yielded samples compatible with AFM measurements have been for charged CNCs, since neutral CNCs formed, for example, by HCl hydrolysis are typically much more extensively aggregated. Both drop casting and spin coating methods with a relatively low CNC concentration (≤0.005 wt%) have been used for deposition on the AFM substrate. One study demonstrated that the spin coating method provided a more reproducible coverage of the surface with a reduced the level of CNC agglomeration,[15] leading to a larger number of individual CNCs per image for size analysis. Another recent study provides qualitative AFM evidence that the level of CNC agglomeration depends on the surface charge which can be modified by the method used to prepare the CNCs or by heat treatment[41] and in agreement with earlier studies on the two-dimensional aggregation of CNCs.[42,43] None of these studies has been able to completely reduce the number of laterally agglomerated CNCs and small clusters, a fraction of which are presumably present in the suspension
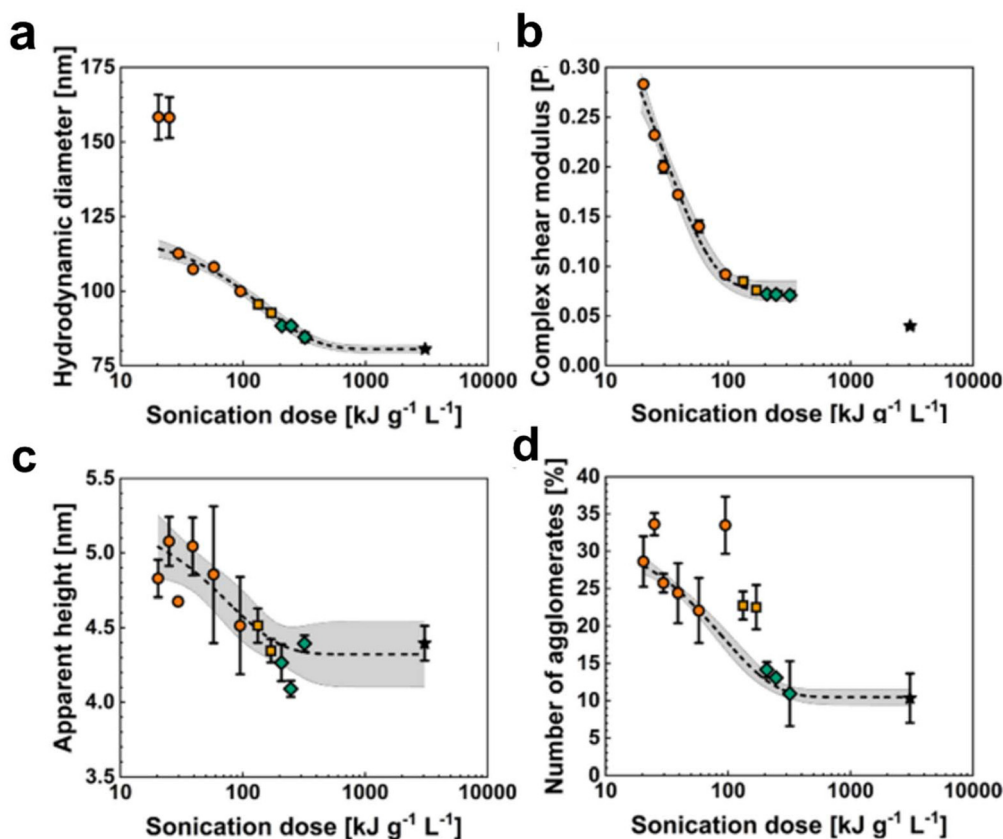

Fig. 2 Plots of DLS hydrodynamic diameter (a), rheology shear modulus (b) and AFM height (c) and number of agglomerates (d) as a function of applied sonication energy. The stars indicate degraded CNCs and the grey shaded areas are the 95% confidence intervals for the line of best fit. This figure has been adapted from ref. 40 with permission from Springer Nature, copyright 2023.

used to prepared the sample. However, several recent studies have started to address the challenges posed by agglomeration either by quantifying the fraction of agglomerates or fractionating the sample as discussed in later sections.

Particle size measurements by AFM

AFM is almost always used to measure particle length and height as a measure of the particle cross section and since the aspect ratio is modest both can be measured using the same image scale. Particle width cannot be assessed by AFM unless a deconvolution procedure is implemented to account for broadening of the feature by tip convolution effects; this adds significantly to the time and effort required and has been done in very few examples.[44,45] Particle length is measured from a cross section drawn thru the long axis of the particle. Height is somewhat more challenging since the particles have an irregular morphology in many cases as illustrated in Fig. 3.[28,34,46,47] Particle irregularity is partly due to the tapered ends of the crystals, but also to the fact that the height can vary by as much as several nm across the long axis of the particle. It is therefore important to note exactly how the particle height is measured, for example at the maximum height along the long axis, but this is rarely included in published image acquisition and analysis protocols. In most cases individual particles as observed by either TEM or AFM are analyzed, but in many cases these particles may consist of individual primary crystallites and particles comprised of several tightly bound crystallites, accounting for the irregular profile and asymmetric cross sections as noted in a number of papers.[2,8,28] However, it should be noted that it may not be straightforward to distinguish between multiple tightly bound crystallites and two adjacent (but separate) crystallites, depending on image quality and resolution and the judgement

of the analyst (see Fig. 3 for examples for both AFM and TEM).[46,48]

Many studies have provided CNC particle size distributions based on imaging a significant number of CNCs (several hundred or more). Some of these have shown differences in size that are attributed to changes in conditions for preparation of the CNCs. However, the size distributions are relatively broad and the level of uncertainty associated with the various measurements is not typically assessed, particularly for earlier studies. Therefore, it is challenging to determine whether or not observed changes are sufficient to conclude whether the materials are the same or different, since this requires consideration of the uncertainty associated with the measurements. This is particularly important if one wishes to assess whether two samples, for example from different suppliers or prepared with different cellulose biomass sources, can be considered the same in terms of their dimensional attributes. Table S1† provides information for CNC particle size distributions from a number of studies for which results are based on a reasonably large number of particles. These studies and other relevant work are discussed below.

A recent VAMAS (Versailles Project on Advanced Materials and Standards) interlaboratory comparison (ILC) under the Nanoparticles Technical Work Area[49] provides data that can be used to address the uncertainty in AFM size measurements of CNCs.[50] In this work CNC suspensions were prepared from a certified reference material[51] in a single laboratory using optimized protocols and then circulated to 10 participating laboratories for AFM imaging and analysis. The participants represented a mix of academic, industrial and government laboratories all of which had extensive experience with AFM and over half of which had prior experience with CNC characterization. The detailed image analysis protocol provided to participants
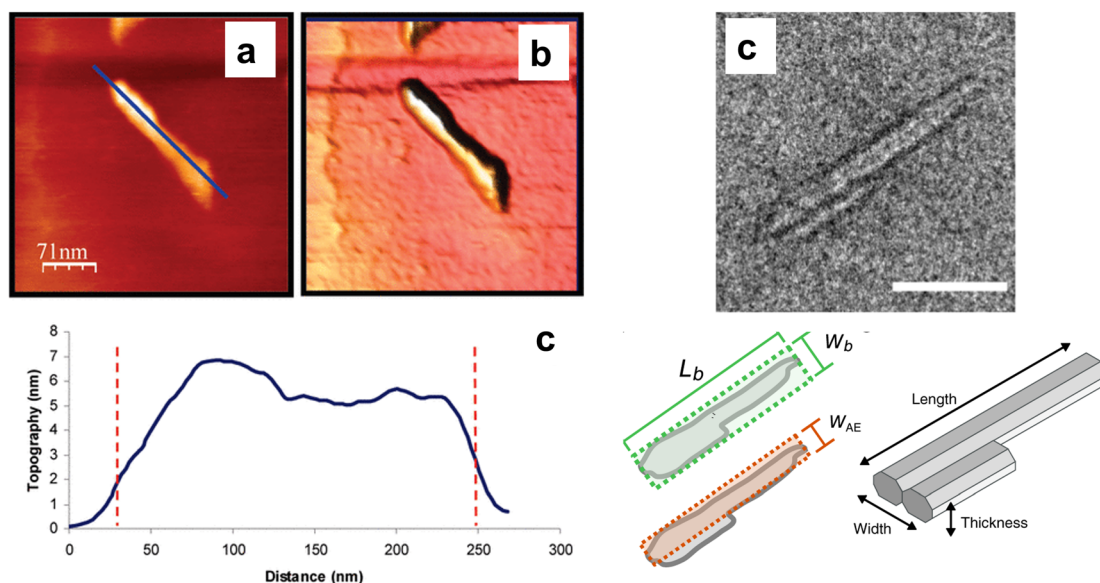

Fig. 3 AFM (a, height; b, phase) images showing a CNC with an irregular height as shown in the line profile below the images. TEM image (c) of an irregular CNC particle comprised of two crystallites with a cartoon illustrating two methods to assess the particle width (scale bar 50 nm). This figure has been adapted from ref. 46 (AFM) with permission from ACS Publications, copyright 2010 and from ref. 48 (TEM) with permission from Nature, copyright 2022.

specified the use of intermittent contact AFM and requested that all identifiable individual particles in each image be analyzed with the height measured at the maximum position along a cross section drawn through the long axis of the particle. There was considerable variation between laboratories in the instruments/probes used, as well as the number of particles analyzed and the reported length and height values. The individual laboratory data sets (Fig. 4a and b) were fit to a skew normal distribution which is characterized by three parameters, a central location (mean), a scale (distribution width) and a shape factor that allows for both positive and negative skew in the particle size distribution. The skew normal distribution becomes a normal distribution for data sets with no asymmetry and can readily accommodate different levels of asymmetry. Note that although a log normal distribution is often assumed for length, the differences in asymmetry in the ILC data sets made the skewed normal distribution a better approach. A similar approach using a pooled data set fit to a skew normal distribution was used to obtain ILC consensus values (Fig. 4c).

The ILC led to final consensus values (±standard deviations as a measure of the breadth of the distribution) of 94.5 ± 39.6 nm, 3.44 ± 1.21 nm and 30.3 ± 12.8 nm for length, height and aspect ratio, respectively.[50] A comparison of the degree of overlap between laboratory values and the consensus estimate for length is shown in Fig. 4d. The study also calculated values for the overdispersion which accounts for the presence of greater variations in the data sets than is expected based on the statistical model and can be used to assess the agreement between the individual laboratory means and the consensus value and to identify potential outliers. Overdispersion values of 15 nm, 0.28 nm and 5.5 were obtained for length, height and aspect ratio, respectively. Note that it may be possible to reduce the uncertainty in measurements if the imaging and analysis are done in a single lab using standard protocols as shown by AFM analysis of multiple samples by two analysts as part of the characterization of the CNC certified reference material that was used in the ILC.[15]

The AFM ILC also provided insight on the effects of using multiple probes to image the samples and on the number of CNCs that should be analyzed to obtain representative results. Since the ILC requested that participants analyze 500 CNCs, 6 of 10 laboratories used multiple probes for imaging. Statistical comparison of the results obtained with individual probes resulted in several interesting observations. First, in one laboratory the particle size increased in a systematic manner throughout the course of imaging, presumably due to wear of the probe used. Conversely for another laboratory a single
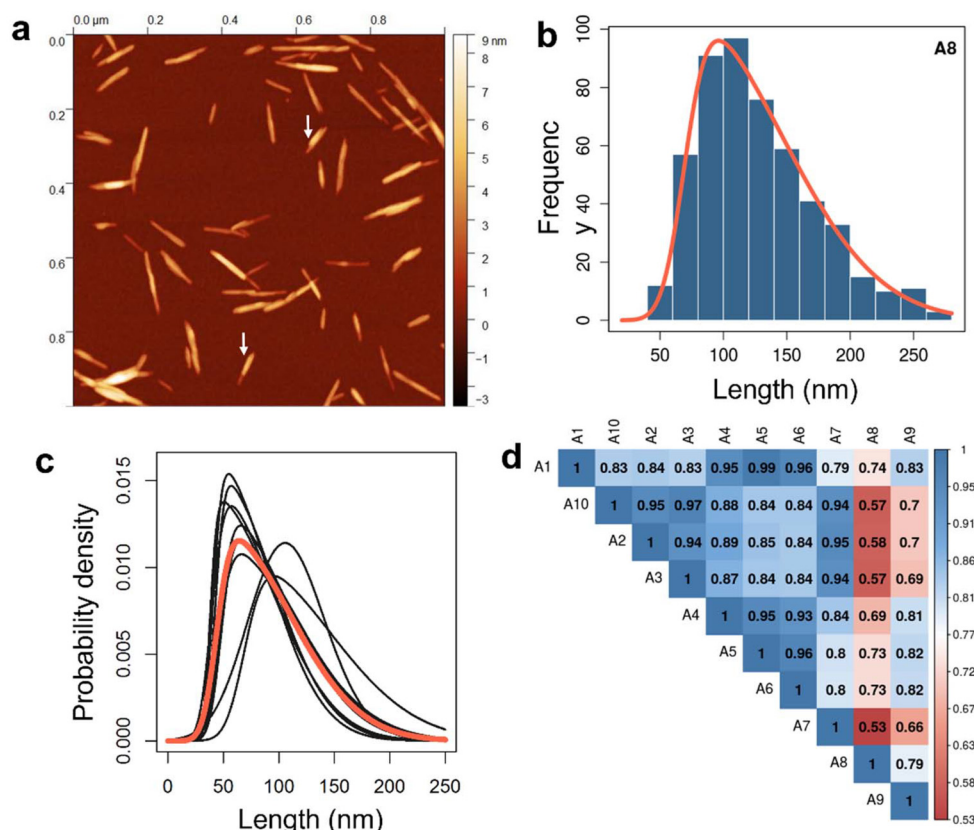

Fig. 4 Results from AFM ILC of CNCs: (a) representative AFM image with arrows showing irregularly shaped particles; (b) length histogram for lab A8; (c) skew normal probability densities for the individual laboratory results (black lines) and the corresponding consensus distribution (orange line); (d) degree of overlap between skew normal length distributions for 10 participating laboratories and the consensus value. This figure has been adapted from ref. 50 with permission from Springer Nature, copyright 2021.

probe was used without any indication that probe wear during image acquisition was a problem. Secondly, the particle sizes measured with different probes were different. The effect was more pronounced for length than height with the variation in length in some cases being comparable to the estimated over-dispersion value of 15 nm for the ILC consensus value. These complexities make it challenging to assess the overall number of particles that should be analyzed for a representative result; however, it was estimated that approximately 300 particles should be adequate for length assuming adequate control of probe performance and imaging, while 200 or 250 particles will give a reliable result for height. Overall, it was concluded that the probe characteristics and potential probe deterioration are significant factors in the observed lab-to-lab variability. Although the variability did not appear to be linked to the probe spring constant, there was evidence that use of a more compliant cantilever for soft tapping mode operation was useful to avoid probe evolution during imaging. Analyst bias plays a small role in the variability based on initial tests of the analysis protocol in multiple labs and earlier results obtained during characterization of the reference material used in the ILC study.[15,50]

The ILC results demonstrate that it is not possible to draw conclusions from small differences in CNC dimensions or aspect ratio for different samples, especially when the experiments are performed in different laboratories, unless one is prepared to accept a relatively large uncertainty. However, it may be more feasible to correlate measured particle size parameters with other properties or performance if the various samples are measured in a single lab with standardized procedures. It is useful to compare the ILC results to recently published studies that examined differences between CNCs prepared by different methods and/or from different sources. The Cranston group has compared properties of a variety of commercially available sulfated or carboxylated CNCs to those of in-house prepared CNCs.[52,53] In the first study only 1 sample had a mean length that was considerably larger than the others (183 nm vs. 132–134 nm) and it is straightforward to conclude that this sample is different from the others (Fig. 5).[53] The heights ranged from 6 nm to 8 nm for the four samples. In a second study the mean length varied from a low of 170 nm to a high of 230 nm, compared to a value of 190 for the in-house CNCs.[52] Although a difference of 40 nm is a clearly significant, it is more difficult to conclude whether a 20 nm length difference is meaningful, given the measured overdispersion value of 15 nm in the ILC. However, this simple comparison ignores several important factors: (1) a lower uncertainty may be obtained for measurements done in a single lab using the same method, (2) the number of particles analyzed in this study (>100) may not be sufficient for a representative result and (3) effects related to differences between probes have not been assessed. Nevertheless, these studies used a number of methods for characterization and even if the dimensional measurements are inconclusive in some cases, the overall conclusions on material similarities are still likely to be valid.
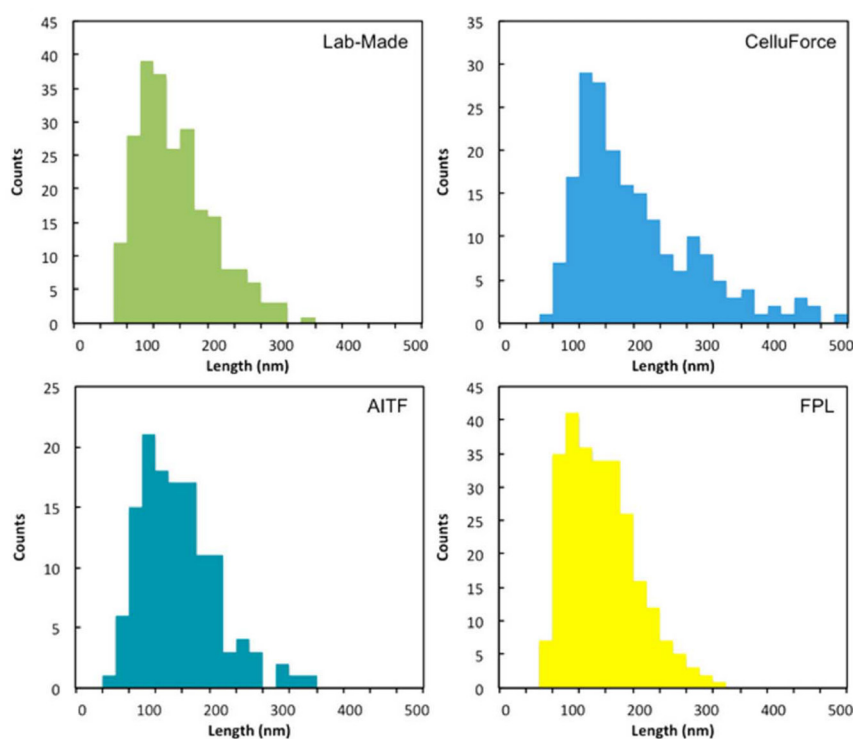

Fig. 5 Length histograms for lab made CNCs and three commercial CNC samples. This figure has been adapted from ref. 53 with permission from ACS Publications, copyright 2017.

In another recent study, CNCs prepared from both wood and cotton using the same procedure were compared.[54] The measured average lengths (based on analysis of ≥250 particles) differed by only 14 nm and this in combination with the standard deviation (60 nm) as a measure of the distribution breadth led the authors to conclude that the length distributions were the same. This conclusion appears reasonable based on the ILC results summarized above. Another paper compared CNCs prepared from three sources, although not with identical preparation methods.[55] AFM height measurements of >1000 CNCs indicated that the diameters were different for bacterial and wood based CNCs but methoxycarboxylated CNCs were not distinguishable from wood CNCs. All three materials had lengths that differed by a minimum of 100 nm, clearly indicating that the length particle size distributions are different. In contrast, a recent overview of the effects of cellulose source and sulfuric acid hydrolysis conditions summarized more than 45 literature papers that used different cellulose sources and gave details on the CNC preparation method and the yield, dimensions and crystallinity of the CNCs.[56] Although the large number of examples is an advantage, this review did not systematically consider how measurements were done and what the possible uncertainties might be. It is clear that small differences in sample dimensions or crystallinity[57] do not allow one to reach any conclusions as to the similarity of the materials. On the other hand, one can conclude that large differences are likely to be meaningful. Nevertheless, this leaves a considerable number of studies where the lack of details and uncertainty assessment makes it challenging to draw any conclusions.

In a final example AFM, SAXS and light scattering data for five sulfated and carboxylated CNCs from cotton and bacterial sources were measured in order to assess the best combination of techniques for accurate measurements of CNC dimensions.[58] The AFM data for length, height and width were based on a minimum of 100 particles and the histograms were fit to a log normal distribution; however, the limited statistics and poor fits for some cases suggest that the number of particles is too small for reliable results. Furthermore, the AFM widths are acknowledged to be inaccurate due to lack of deconvolution and aggregation of particles. The authors concluded that a combination of AFM measurements to assess the mean length and polydispersity and SAXS to measure lateral dimensions was preferable. However, both AFM height and width (inaccurate due to lack of deconvolution) are larger than values obtained by SAXS, although the width/height ratios for each sample are similar for the two methods. The limited number of particles analyzed by AFM and the variations in measured cross sectional values do not provide strong support for the conclusions on the optimal methods for dimensional measurements.

TEM of CNCs

There are fewer examples where TEM has been used to obtain morphological and dimensional information for CNCs. Similarly to AFM, the propensity of these materials to aggre-

gate and agglomerate is an issue but, in addition, they are prone to electron beam induced damage and the EM contrast is limited for carbon-rich materials. The limited contrast means that most studies have imaged metal-stained samples. Studies up to approximately 2015 are covered in various reviews[2,27,59] and indicate that almost all EM studies of CNCs that provide detailed dimensional analysis are done using TEM with samples deposited on carbon-coated copper grids that are pretreated by glow discharge or plasma cleaning to render them more hydrophilic, followed by staining with uranyl acetate.

Several recent papers considered approaches to optimize sample preparation and imaging conditions to obtain the most reliable results for CNCs[59,60] and CNMs.[61] The Foster group tested a number of methods to obtain better dispersed samples and concluded that use of a never-dried CNC suspension with added bovine serum albumin and deposition on silicon oxide coated Formvar grids was the optimal method.[60] They also examined different stains, concluding that methylamine vanadate provided somewhat better results than other stains such as uranyl acetate, ammonium molybdate, iodine and methylamine vanadate. More recently TEM imaging has been used to optimize uranyl acetate staining with the conclusion that the sample drying method and grid conditions were the most significant factors in obtaining images with adequate contrast and minimal aggregation that are suitable for particle size analysis.[62] The conclusions of these studies were based largely on a qualitative assessment of CNC dimensions and dispersion level. More recently the effects of grid type, grid pre-treatment and negative staining were examined using TEM imaging with calculation of fractal dimension and lacunarity using ImageJ as a measure of assessing the aggregation/dispersion and the degree of fibrillation.[63] It was concluded that formvar/carbon coated grids coated with PLL gave optimal reproducibility, although it is not clear that the samples studied are suitable for size and shape analysis of individual CNCs. The same sample preparation method was subsequently used to examine the aggregation state of CNCs as a function of increased sonication times, again using TEM imaging for analysis.[38] Five types of clusters were identified, with the fractional amount of each changing with applied sonication energy; it was concluded that the approach showed promise for assessing the aggregation state of CNCs.

The ILC referred to above that tested an AFM protocol for obtaining particle size distributions for CNCs also examined TEM imaging and data analysis methods.[64] A similar approach was used for TEM with an optimized sample preparation method developed by the piloting lab and used to prepare the ILC samples. After examination of a variety of factors, the final method involved deposition of a dilute CNC suspension on carbon-coated copper grids that had been plasma-cleaned, followed by washing and staining with a 2% solution of uranyl acetate. Note that this still led to considerable variability in the density of CNCs across the grid, although it was possible to find areas with a reasonable particle density and less agglomeration. Ten laboratories participated in this ILC and all
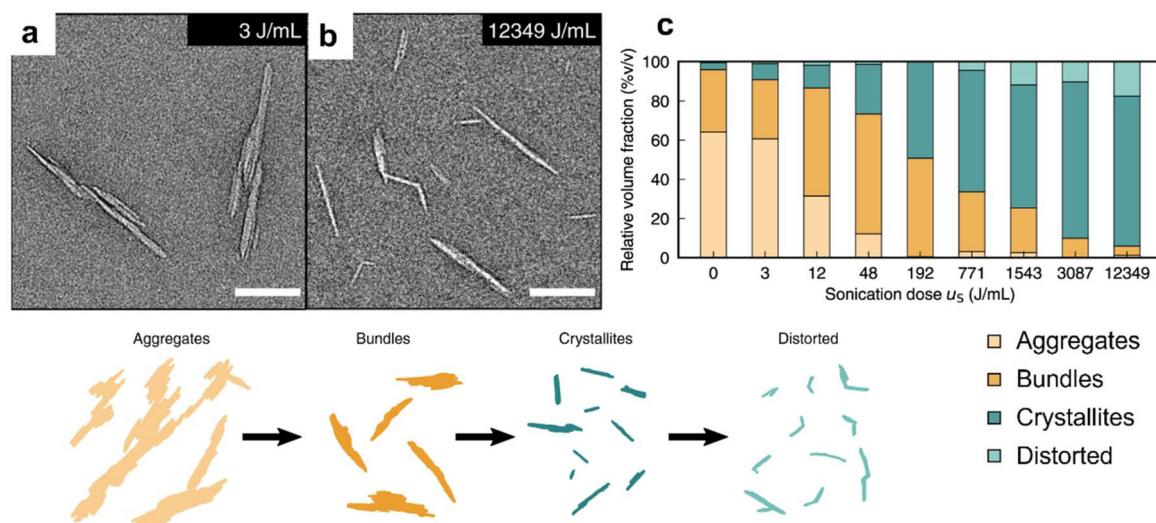
Fig. 6 TEM images (scale bar 100 nm) for CNC samples sonicated with low (a) and high (b) energy, with the cartoon under the images illustrating the different observed features. Panel (c) shows the fraction of each of four particle types: (aggregates, bundles of laterally associated CNCs, crystallites and distorted particles) as a function of the sonication dose. This figure has been adapted from ref. 48, with permission from nature, copyright 2022.

returned data sets. As for the AFM study, this ILC tested microscopes from several of the main manufacturers and most participants followed the recommended protocol. However, there was still considerable variation between laboratories in the mean length and width reported and in the overall shape of the particle size distributions. The same approach of fitting to a skew normal distribution was followed, leading to final consensus values (±standard deviation as a measure of the distribution breadth) of 95.8 ± 39 nm, 8.6 ± 2.9 nm and 13.3 ± 5.7 for length, width and aspect ratio, respectively, with overdispersion values of 12.3 nm, 0.78 nm and 1.8. It was concluded that the selection of individual CNCs for analysis and the variability in CNC agglomeration and staining are the main factors that lead to variations in measured length and width between laboratories.

TEM has been used less frequently recently for comparison of different materials. In one case it was used to examine the effects of the acid hydrolysis conditions on the properties of CNCs generated from eucalyptus pulps.[65] A decrease in the length-weighted average length from 280 nm to approximately 120 nm was observed for an approximately 10% increase in acid concentration. Although the number of CNC analyzed was as low as 50 for samples with a low CNC yield, up to 350 particles were analyzed for other samples; given the large variation in length, the overall conclusions make this paper a valuable illustration of the ability to tailor the CNC properties by varying the hydrolysis conditions.

A very recent study has used detailed morphological analysis of TEM images to investigate the mechanism for transfer of chirality from the molecular to the colloidal scale for CNCs.[48] CNC suspensions were sonicated with increasing energies and the evolution in particle size and shape were evaluated from TEM images for a minimum of 250 CNCs per sample; the irregular shape of the particles was assessed by measuring an area equivalent width (W_{AE}) which better represents the average width of an irregularly-shaped elongated particle (Fig. 3). Analysis of the W_{AE}, length and aspect ratio as a function of sonication energy (Fig. 6) allowed separation of the analyzed features into four different "particle" classes: aggregates are disordered assemblies of small crystallites; bundles are laterally connected crystallites (*i.e.*, connected along their long axes); individual crystallites are small regular rod-shaped crystallites; distorted (often kinked) particles appear at higher sonication dose and are judged to be mechanically damaged (Fig. 6a and b) by excessive sonication. Correlation of the changes in the fraction of the particle classes at different sonication energies (Fig. 6c) with the formation and properties of chiral CNC films produced from the same samples led to the conclusion that the particle bundles act as chiral dopants, allowing for transfer of chirality from the molecular to the colloidal scale. This paper provides an impressive example of using detailed morphological analysis of CNCs to provide fundamental information on the factors that control the chiral properties of CNC films, an important factor for optical film applications.

Comparison of AFM and TEM dimensions

A few papers have reported both AFM and TEM data for the same CNCs.[15,34,64,66] The ILC work referred to above used a certified reference material for all measurements and obtained good agreement for CNC length, with <1.5 nm difference in the mean length for the two methods.[64] However, the agreement between AFM and TEM for CNC length obtained in the ILC can be contrasted to the earlier characterization of the CNC reference material for which mean lengths were lower for both methods and differed by 10 nm (AFM 77 nm, TEM, 87 nm).[15] This data set was based on measurement of five independently prepared samples with two analysts for each

AFM image set and TEM imaging by two laboratories. Considering the variation observed between laboratories in the ILC and the estimated overdispersion for each method, one cannot conclude that the 10 nm difference is significant. Interestingly, an earlier study of a similar CNC from the same commercial source also observed an approximately 10 nm difference between AFM and TEM, in this case with AFM giving the higher value.[34] The large number of data sets for the CNC reference material demonstrates that the same length can be obtained by either method, although a large number of determinations are required to converge to a constant value, highlighting the importance of understanding the uncertainties associated with individual measurements.

By contrast to the above observations for length, a number of studies have reported that the measured TEM width is larger than the AFM height by a factor of ≥2. One of the first direct comparisons was by Nishiyama and coworkers who reported that TEM width was 2–4 times larger than AFM height for CNCs prepared from cotton, avicel and tunicate.[28] The differences between the height and width were attributed to flat, ribbon-like particles that were comprised of multiple individual crystallites. Similar conclusions were reached for CNCs with a cellulose II structure, several wood-derived CNCs and the CNCs used in the AFM/TEM ILC.[47,67] However, a number of microscopy studies have indicated that the number of lateral agglomerates varies with sample preparation conditions, consistent with SAXS/SANS studies[68,69] which concluded that CNCs in suspension are laterally aggregated in a concentration dependent manner. It may be difficult, if not impossible, to distinguish between such lateral particle agglomeration and the presence of individual particles comprised of two or more tightly bound crystallites that appear as a single (irregularly-shaped) particle.

The comparison of height and width has been examined in more detail recently by Chen and coworkers using a single method so that width and height are measured for the same particles.[44] CNCs were initially fractionated by asymmetric field flow fractionation (AF4) using either semi-preparative or analytical conditions and the collected fractions were analyzed by AFM. The initial AF4 fraction was shown to contain predominantly single CNCs (up to 90% of particles), and the fractions of laterally associated "dimers" and small clusters increased significantly in later fractions (Fig. 7).[70] This work demonstrates that the CNC clusters that are typically observed in samples deposited for AFM can be almost completely eliminated by fractionation and indicates that a fraction of the dimers and clusters are pre-existing in the suspension, rather than being formed during the deposition process.[70] Several previous attempts at CNC fractionation had been reported to reduce polydispersity, but not to the point of producing fractions with predominantly single CNCs.[71,72] The use of a carefully optimized AF4 separation method and a starting CNC suspension that was less polydisperse than those used in earlier work, along with detailed AFM interrogation of individual AF4 fractions, provided a significant improvement in the Chen study.

In a follow-up paper a fractionated CNC suspension was codeposited with 10 nm gold nanoparticles and imaged by AFM.[44] The gold served as an internal calibrant to measure tip size for each image and to facilitate deconvolution of the observed CNC width. This analysis led to the conclusion that CNC particles showed a range of widths with approximately a third of particles having a width that was similar to the observed height, the remainder having widths in the same range as TEM and consistent with laterally associated particles. These findings are consistent with the earlier studies of larger cotton derived CNCs that also showed a rectangular cross section and with an early attempt to obtain the deconvoluted width of wood-derived CNCs.[28,69]

Another recent study reported both AFM and TEM data for CNCs from two commercial sources. The TEM length (142 nm) differed from the AFM length (118 nm) by 24 nm for one of
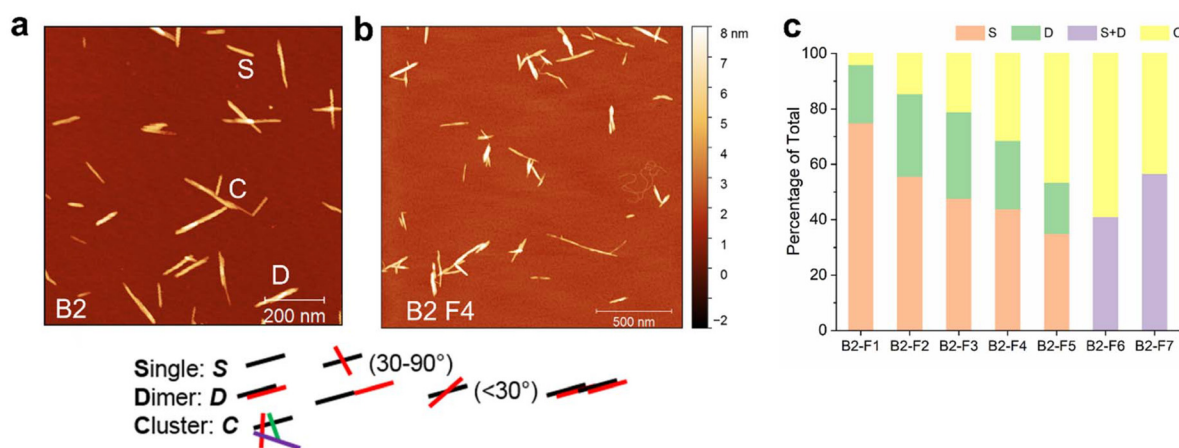

Fig. 7 Representative AFM images showing the number of single, dimer and clustered CNCs for two AF4 fractions with an illustrative cartoon under the images: (a) fraction 1, (b) fraction 4. Panel (c) shows the change in the percentage of single, dimer and cluster CNCs for the AF4 fractions. This figure has been adapted from ref. 70 with permission from Springer Nature, copyright 2019.

the two samples but only by 12 nm for the other (89 *vs.* 101 nm).[66] The AFM heights (4.3 nm, 4.9 nm) were also smaller than the TEM widths (6.2 nm and 12.8 nm) and the differences were hypothesized to be caused by differences in image resolution. Although the TEM width is probably less accurate due to the relatively poor image contrast and a lower image resolution than for AFM height, it also seems likely that lateral aggregation is a contributing factor, particularly for the sample with larger width. It is noteworthy that one might conclude on the basis of only the TEM data that the two samples had different particle size distributions whereas the AFM differences are not large enough to draw such a conclusion. The number of particles analyzed is also small for AFM, and considering the likely uncertainties, additional data may be necessary for a definitive conclusion on the similarity of the dimensions of the two materials, although a *t*-test did indicate a statistical difference between them.

Individual cellulose nanofibrils

There are several differences between iCNFs and CNCs: iCNFs are typically longer with frequent kinks or bends along their long axis, they have a relatively symmetric width of ~3 nm (based on TEM), since they are comprised of individual elementary fibrils and their length varies from ~200 nm to 1 µm or larger.[12,13] Note that these dimensions are for wood-derived iCNFs. The early studies from the Isogai group on the development of the TEMPO-oxidation method used to produce iCNFs employed TEM for qualitative size and morphology analysis.[12,13,73] The term iCNFs has recently been defined by ISO to distinguish this important and morphologically distinct subset of CNFs but has not yet been widely adopted or utilized in the literature.[10] Papers often refer to TEMPO-CNF, TOCN or sometimes CNFs, although it is clear that the preparation method involves TEMPO oxidation. Although particles with straight sections connected by occasional kinks are typical for iCNFs, slight curvature has been observed in some cases for wood-derived iCNFs,[73,74] as well as for tunicate iCNFs[75] which have larger cross sections that reflect the different size of the elementary fibril.

Sample preparation

Recently most detailed microscopy studies of iCNFs have used AFM.[16,29,76–81] Several different methods have been used to prepare samples, including (1) deposition on mica, rinsing and drying and (2) deposition on APTES-modified mica or silicon wafers that were oxidized to give a silica surface or modified with polymer; typically a dilute solution of iCNFs was used (≤0.001 wt%). The results show a variety of particle densities on the surface, but in general one can conclude that it is reasonably straightforward to obtain well-separated individual particles. Most studies have used tapping mode to acquire images, although details on the AFM mode and method for image analysis are lacking in some cases. Several groups have used peak force tapping mode for either nano-

mechanical measurements or for optimal high resolution imaging.[29,75]

AFM and TEM studies of iCNF

Several AFM studies have focused primarily on iCNF height. In one case heights between 2.0 and 2.9 nm were obtained for iCNFs prepared with differing amounts of charged carboxylate groups.[16] The AFM measurements of cross section were correlated with turbidity measurements of the same samples, indicating that turbidity can be used as a rapid means of estimating iCNF cross section.[16] In another study the iCNF height was measured at the highest point on straight iCNF sections with no obvious twist for 13 samples prepared with varying levels of Tempo oxidant and mechanical treatment.[76] The height values showed little variation, all being in the range of 2.4–2.6 nm. Both studies analyzed only between 50–100 particles, but this may be adequate since the height size distribution is narrow. Another recent AFM study provided width measurements (*n* = 200) of two iCNFs generated by Tempo-mediated oxidation.[82] However, the large width (~20 nm) is not useful in the absence of deconvolution. Finally, a study that correlated particle aspect ratio and surface charge with formation of colloidal glasses or glasses has concluded that iCNFs with low and high surface charge have the same diameter (2.9–3.3 nm), based on AFM measurement of the height of >1000 particles; however, the length decreases by approximately a factor of 4 with increasing surface charge.[55] See Table S2† for additional information on the more detailed studies.

One study used a combination of AFM to measure iCNF height and TEM to measure length and then correlated aspect ratio and surface charge density with flow properties and flocculation behavior, important factors for high performance materials containing CNMs.[77] The results showed that the particle thickness distribution (*n* = 150) was similar for 4 samples (means of 2.1 to 2.5 nm) with charge density varying from 380 to 1360 µmol g^{-1} but that the TEM length (*N* = 200) decreased from ~650 nm for low charge to ~420 for the highest surface charge. In this case the dimensions were compared to those estimated from SAXS data using a ribbon model, which gave values for the smaller cross section of 2.2 nm and for the larger between 4.3 and 5.9 nm in reasonably good agreement with a qualitative assessment of TEM width (~8 nm). This is one of few studies that attempts to measure the two cross-sectional dimensions of iCNFs from the same sample. Although the results suggest an asymmetric cross section, it would be important to verify that the TEM resolution is adequate for width measurements. However, the results are consistent with previous studies which concluded that elementary fibrils of plant-derived cellulose have a slightly asymmetric cross section.[83] The results were correlated with the rheological behavior of iCNFs, providing insight on the critical networking point, which is relevant to high-performance CNM-based materials.

The Nyström and Mezzenga groups reported a detailed AFM study of iCNFs with a comparison to wood CNCs generated by HCl oxidation of Tempo-CNFs and bacterial CNCs gen-

erated by sulfuric acid hydrolysis.[29] The three samples showed that all fibrils and crystals (Fig. 8a and b) with observable chirality were right-handed in AFM, cryo-SEM and TEM images, independent of imaging mode. Measurement of the mechanical properties demonstrated that iCNF had Young's modulus in the range of 20–50 GPa, similar to both wood and bacterial CNCs, suggesting that the mechanical properties do not vary with the sample preparation method. Careful analysis of the distribution of kink angles for iCNFs (Fig. 8c) indicated that the observed kinks result from mechanical treatment during sample preparation, rather than from the presence of amorphous regions of the fibril. Histograms for the size distribution (Fig. 8d and e) obtained from analysis of 2380 individual iCNFs showed that the average length was 511 nm, based on a log normal fit. The lengths were measured by tracing the entire length of the particle with a custom routine that accounted for different kink angles. The height distribution was symmetric with values in the range of 1.9 nm–2.7 nm with the most probable height of 2.35 nm and no obvious difference between values obtained in straight and kinked regions of the fibril. Some splits were observed in individual fibrils, possibly accounting for the relatively broad range of heights. Finally, it was possible to visualize very thin features that were hypothesized to be individual cellulose chains. Similar features have been reported in a later study.[76]

Another study from the Nyström and Mezzenga groups has examined the effect of sonication on the total fibril length, the number of kinks per fibril and the length of straight segments.[80] A combination of AFM image analysis and statistical considerations led to the conclusion that sonication causes breaks along straight segments, not at pre-existing kinks. Acid cleavage of iCNFs to give carboxylated CNCs occurs preferentially both at kinks and in between kinks. This study also

demonstrated that the initial right-handed chirality of the iCNFs is inverted when a cholesteric phase is formed from carboxylated CNCs generated from iCNFs.

The above study was extended to a more detailed examination of the structural properties of iCNFs generated from softwood pulp as a function of production parameters, including bleaching, extent of oxidation and sonication.[79] A higher surface carboxylate content had previously been shown to yield shorter iCNFs as evidenced by decreases in both fibril length and degree of polymerization (determined from viscosity measurements) for more highly oxidized fibrils.[81] The samples were prepared by deposition on APTES coated mica, followed by rinsing and drying and imaged in tapping mode and only single fibrils were considered although a comparison showed that ignoring agglomerates and split fibrils introduced only minor changes (<3%). Analysis of >200 iCNFs for various conditions demonstrated that increased sonication time and increased surface charge both led to shorter and thinner fibrils with fewer kinks, with an optimum in terms of maximum length and minimal kinks for samples with approx. 600 µmol g^{-1} charge density. The fibril twisting periodicity was also shown to decrease with higher charge density, consistent with expectations based on electrostatic repulsion.

A recent study from the Willhammar and Saito groups has used AFM in combination with other methods to examine the local crystalline structure and twisting in tunicate iCNFs.[75] A combination of scanning electron diffraction and AFM were used to demonstrate that the crystalline structure of the iCNFs was maintained as the fiber twists. Furthermore, the twist rate was found to be proportional to the inverse of the cross-sectional area and both methods gave similar twist rates of 0.24 and 0.26° nm^{-1}. Of particular interest from the point of view of image analysis this paper used an automated method
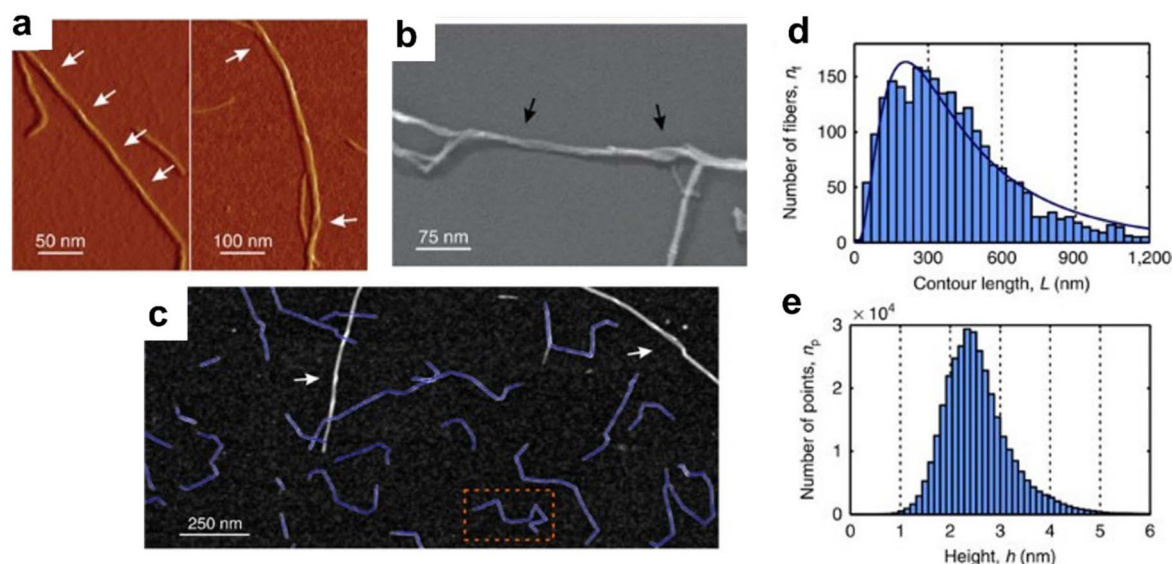

Fig. 8 AFM (a) and TEM (b) images of iCNFs showing the right-handed chirality and an AFM image (c) that shows tracking of the length of a number of kinked fibrils. Length and height histograms for iCNFs are shown in panels (d) and (e). This figure has been adapted from ref. 29 with permission from Nature, copyright 2015.
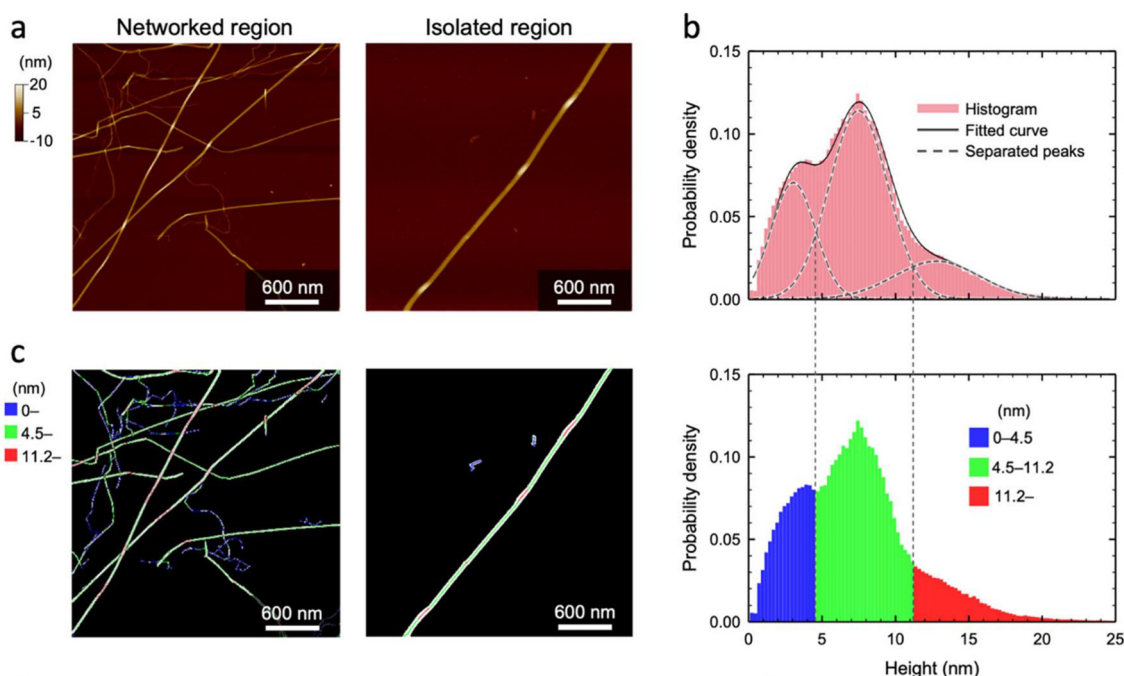
Fig. 9 AFM images of networked and isolated areas of tunicate iCNFs (a) and histograms (b) that are fit to three Gaussian functions (top) and separated into three size groups (bottom). The three different sizes are indicated in blue, red and green in the AFM images in (c). This figure has been adapted from ref. 75 with permission from ACS Publications, copyright 2021.

implemented in Python to determine the particle height, leading to a histogram that could be modeled as three normal distributions. It was concluded that there were extended iCNF regions with a consistent thickness of 3.0 ± 1.5 nm while twisted regions were thicker (7.4 ± 2.0 nm), Fig. 9. The third component was assigned to overlapping iCNFs (13.0 ± 2.9 nm). In a related TEM and electron microdiffraction study the intrinsic right-handed twisting of tunicate CNCs has been observed under cryogenic conditions.[84]

Cellulose nanofibrils

CNFs are considerably more challenging for microscopy measurements since they are typically complex structures with a branched or tree-like structure that has fibrils with a range of sizes (Fig. 1c). As a result, there are so far relatively few detailed studies of their size and morphology and no general consensus on how to deal with the complex sample morphologies with many interconnected branches as well as individual fibrils that are separated from the larger structures.[85] For most sample morphologies it is feasible to measure the fibril width and mean values can vary from <10 nm up to 60 nm or larger, with the smaller fibrils having similar widths to CNCs and iCNFs. Length measurements are more challenging and it may be necessary to record images on several length scales to capture both dimensions; for some samples the extent of interconnectedness may preclude detailed length measurements. Although many CNF have interconnected

structures with curved particles/branches and sharp angles at nodes where one branch is connected to a larger one, the morphology varies considerably with the level of sample processing and the cellulose biomass source. More highly processed CNFs may exhibit a significant number of smaller fibrils that are either curved or have occasional kinks along the long axis of the fibril,[86–88] somewhat similar to the morphology of iCNFs. Overall, these observations and the above comments on CNC and iCNF morphology suggest that the generalization of straight (CNCs), kinked/straight (iCNFs) and branched, curved (CNF) morphologies is typical of many CNMs but does not apply to all samples. This presumably reflects a combination of the dimensions of the initial elementary fibrils assembled by the enzyme complex for CNMs from different biomass sources, the assembly of these fibrils into larger structures, the disassembly of the cellulose microfibrils into smaller CNM particles and the energy input to redisperse the particles, if necessary.

Sample preparation

CNFs have been produced by a range of different methods starting with many different sources of cellulose biomass, making it difficult to compare the utility of sample preparation methods across different studies. These issues are compounded by the observation that the details provided for sample preparation, imaging and data analysis are not sufficient to allow for reproduction and comparison to other studies. A common theme for sample preparation is that sample dispersion can be maximized by starting with dilute

CNF suspensions (*e.g.*, 0.001 wt% in water) that have been pre-treated by vortexing or sonication to minimize aggregation. Another commonly used strategy is deposition of the sample on PLL or polyethyleneimine coated substrates such as mica or silicon in order to minimize particle–particle interactions.[87,89,90] Preparation of samples by freezing and subsequent lyophilization has also shown promise as a method to minimize any possible redistribution and agglomeration during sample drying on the substrate and to maintain as much as possible the sample organization in the original suspension.[17,89] In cases where a relatively small amount of mechanical energy is used to generate CNFs, it may be advantageous to fractionate the sample by either centrifugation or screening to remove large fibers prior to SEM analysis.[14,91] With few exceptions samples have been coated with a thin metal layer to provide adequate contrast. However, a promising alternative to metal coating is the deposition of samples on a conductive support which facilitates negative contrast imaging and has been shown to give superior contrast to that typically obtained for metal coated samples.[87,92]

Electron microscopy studies

By contrast to microscopy studies of CNCs and iCNFs which have used AFM and/or TEM, SEM of CNFs has generally been used to provide a qualitative assessment of the overall morphology and dimensions of the sample; size measurements based on analysis of a sufficient number of particles are rare, even for examples where good quality images with reasonable levels of sample dispersion have been achieved. Here we focus on recent studies in which SEM and occasionally TEM have been used to obtain morphological and dimensional information on CNFs. Two early papers provide a good overview of the types of structures that are typical of CNFs.[17,93] In one case, a combination of SEM and TEM was used to measure diameters of fibrils, with values that range from approximately 5 nm to 300 nm.[93] Note that this work provides few details on exactly how the various measurements are done, for example the number of CNFs analyzed and how diameter is measured. Nevertheless, both papers provide a good overview of the challenges associated with analyzing CNF diameter. Work by Larsson and colleagues also provides an excellent illustration of the different morphologies that are observed for two samples of microfibrillated cellulose with differing degrees of fibrillation.[14] A combination of filtration and centrifugation was used to separate each sample into four fractions of varying size and mass fraction. Although these materials have a relatively small nano fraction (10–20% by mass), their characterization by TEM and surface charge measurements provides a good illustration of the complexity of fibrillated CNMs.

Literature reports with particle size distributions for CNFs are summarized in Table S3† and discussed below. Two papers from the Demokritou group also used a combination of SEM and TEM to analyze the diameter of CNFs, in one case for samples that have fewer interconnected fibrils, facilitating the analysis.[89,90] This work found fibril widths in the range of 50–80 nm for several samples and also reported that depo-

sition of CNF suspensions in cell culture media gave samples that were less satisfactory for imaging. One interesting aspect of these studies was the attempt to measure fibril length and to deal with the interconnected fibrils by assessing the distance between branches (node-to-node length of 336 ± 233 nm) as well as the average length (6.71 ± 5.6 μm) of single fibrils. This is a potentially interesting approach for dealing with the structural complexity of CNFs, although there are insufficient details to allow the approach to be generalized.

One of the most detailed studies to date of CNF particle size was reported by the Batchelor group.[86] This study examined the effect of analyst bias and number of particles analyzed for two samples with differing degrees of heterogeneity/ fibrillation generated from eucalyptus pulp. Samples were coated with iridium to improve contrast, resulting in high quality images with a relatively large number of branched particles. The CNF width varied from around 5 nm to around 200 nm with some variation depending on the analyst, the number of particles analyzed and the sample; the median fibril width was typically between 25 to 30 nm (Fig. 10). It was concluded that it is preferable to measure all analyzable particles in an image to reduce analyst bias and that approximately 150 fibrils should be analyzed to obtain a representative result. One of the main strengths of this study was the careful data analysis and the evaluation of whether observed differences were statistically meaningful. However, some details on the location at which fibril width was measured are lacking.

The approach described above is similar to a previous study by the same group on the effect of refining and homogenization on the production of nanocellulose.[94] Low and high magnification images were used to track the fiber width by SEM on two length scales as a function of refining and homogenization, with the most extensively processed sample being similar to that used in the above work. The SEM data was combined with gel point determination by sedimentation to estimate the aspect ratio. The study concluded that there is only a small benefit on the mechanical sheet strength for the tenfold increase in the energy consumption required to produce very low diameter (12 nm median), high aspect ratio (229) fibers. The use of SEM with images on two length scales was also used more recently along with specific viscosity measurement from rheology and aspect ratios from AFM to compare CNMs with particles of three distinct sizes, CNCs, CNFs and wood fibres.[95] This work highlights the utility of careful microscopy measurements with attention to multiple image scales, adequate numbers of analyzed particles and statistical analysis to assess the applicability of complementary methods for obtaining information on dimensional parameters.

Other microscopy approaches

Few papers have used AFM to assess size and morphology of CNFs, despite its relatively common use for examining CNCs and iCNFs. This is largely because the complex entangled structures typical of CNFs are challenging for AFM imaging as noted in a recent overview of the priorities for CNF particle
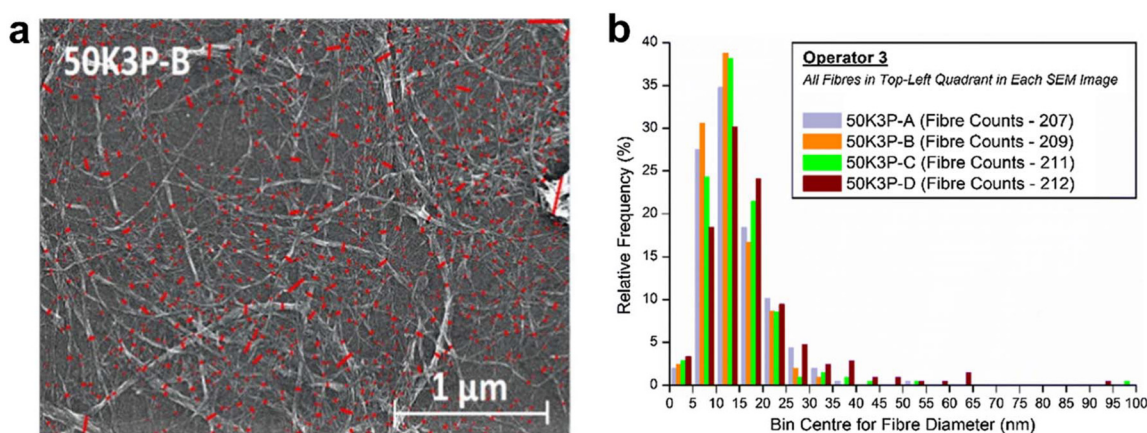
Fig. 10 Representative image of CNFs, annotated to show the fibrils counted (a, red lines) and a histogram showing the width distribution measured by a single analyst for this sample for each of four images (b). This figure has been adapted from ref. 86 with permission from Springer Nature, copyright 2020.

size measurements.[85] The first issue is that the fibril length is hard to measure and may well require images on multiple length scales due to the high polydispersity of the sample. The second issue is that the presence of small individual fibrils and large bundles of fibrils leads to large variations in z-scale within an image that makes it difficult to adequately assess the height of both small fibrils and large fibril bundles. Scan times are also typically considerably longer than for EM and tip convolution effects mean that it is not feasible to measure accurate widths of smaller fibrils, compounding the difficulty. Despite these challenges several recent papers have used AFM for size analysis of CNFs. One study demonstrated that APTES-coated silica is a good choice for immobilization of CNFs for sample preparation for AFM.[96] In another study CNFs were used to achieve high brightness in very thin films that were only a few micrometers thick.[88] Birch pulp CNFs were fractionated by differential centrifugation to give 3 sizes of fibrils (fine, medium and coarse) that were deposited on a microscope slide and their thickness assessed by AFM height measurements of >500 CNFs particles per sample.[88] Histograms were fit with a log normal distribution which gave thicknesses (sd) of 4.2 nm (2.7), 5.6 nm (3.2) and 19.5 nm (13.2), although details on which CNFs were analyzed and where on the CNFs the heights were measured are not provided. The two smaller fractions cannot be concluded to differ in thickness, given the likely uncertainty of the measurement, but the coarser fraction is certainly of different size.[88] A recent study that used CNFs to reinforce polymer films measured heights and lengths of particles by AFM, reporting values of ~1.2 μm and 38.8 nm, although with limited detail on measurement procedures.[97]

Work by Mattos *et al.* has attempted to resolve some of the issues associated with using AFM to characterize particle sizes for CNFs and has also compared results to those obtained by negative contrast SEM.[87] They studied CNFs with an intermediate degree of fibrillation and considered effects related to flattening of the CNFs on the surface, leading to relatively large

differences between height and width that must be accounted for in determining the CNF cross section and aspect ratio. CNFs were deposited by immersing poly(ethylene imine)-coated mica in a dilute CNF solution and imaged in tapping mode with 500 randomly selected particles analyzed for width and height measurements. Note that there was significant agglomeration for CNFs, limiting the number of individual CNFs for size analysis. Values of AFM height and width varied significantly: 6 ± 3 nm and 67 ± 18 nm, respectively. This was partly due to tip convolution effects but even after correction using the nominal tip characteristics, the AFM widths were still substantially larger than height, leading to the hypothesis that flattening as well as aggregation of CNFs contribute to the observed effects. Consistent with this AFM of CNFs on bare mica showed reduced widths. Here it is worth noting that asymmetric particle cross sections have been hypothesized for various CNMs using other methods and have also been confirmed experimentally for CNCs. It is therefore still to be determined how much of the difference between width and height in the present example can be attributed to flattening of the CNFs on the surface.

The Mattos study compared AFM to negative contrast SEM with CNFs deposited on gold coated mica and demonstrated that this method had significantly improved contrast compared to conventional SEM with metal coating of deposited CNFs (Fig. 11). SEM widths were correlated with AFM height and width. A second recent study has used negative contrast SEM on a conductive silicon substrate to obtain SEM images of several CNF samples as a function of dewatering treatment. This work recorded images on three different magnifications to capture the CNF complexity and also analyzed large numbers of particles, giving statistically relevant data sets. The width was measured at each branch point as illustrated in the annotated images provided as supporting information of the paper. Mean or median widths were not calculated from the histograms. In another example, AFM height and SEM width (conventional SEM with gold coated samples) were measured
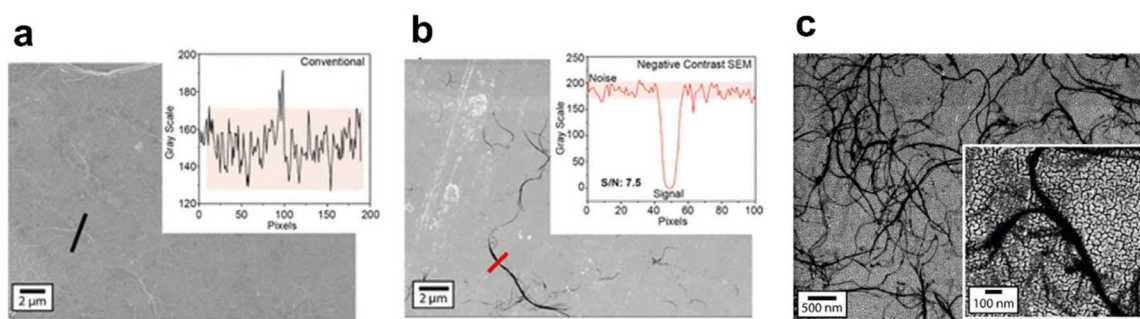
Fig. 11 TEM images illustrating the difference in contrast for conventional imaging of CNFs deposited on a substrate and then coated with metal (a) and CNFs deposited on a metal-coated substrate (b, negative contrast imaging). Image (c) shows a number of interconnected CNFs, illustrating the variation in morphology. This figure has been adapted from ref. 87 with permission from ACS Publications, copyright 2019.

for CNFs generated from agricultural waste; similar estimates for the fibril cross section were obtained for each method, although the histograms provided are broader for AFM.[98]

Two recent papers have used fluorescence microscopy alone or in combination with EM to examine dimensions of CNFs.[99] Tagawa and coworkers imaged dye-stained CNFs generated by an aqueous counter collision method and deposited on transparent polymer films using a combination of AFM and fluorescence microscopy. They obtained similar average lengths from each method for each of four samples (average lengths varied from 1 to 4 μm) that were generated from different cellulose biomass sources. Of particular interest in this study was the comparison of CNFs widths from SEM and optical microscopy, demonstrating that isolated CNFs with widths down to approximately 20 nm can be detected by fluorescence for well-dispersed samples with fibrils separated by several hundred nm. This study highlights the possibility of using optical/fluorescence microscopy to obtain dimensional information (length) over a wider range of image scales than is currently used with optical microscopy, although not with the resolution needed to detect the smallest fibrils present in most CNF samples or for samples with densely packed and interconnected fibrils. Super-resolution imaging has also been used to detect dye-labelled CNFs, a technically challenging experiment, although one with limited applicability.[100]

Studies comparing different CNMs

There are a few literature studies where more than one type of CNMs has been studied using similar methods and approaches and several examples are noted above. Some papers provide qualitative image analysis confirming the general observations concerning the morphology and size for the three types of CNMs. In one early study a combination of AFM height and TEM length for a minimum of 200 particles per sample was measured for three CNCs prepared with different reaction times and compared to CNFs prepared by mechanical defibrillation and iCNFs prepared by TEMPO oxidation.[101] The particle heights decreased for CNC (from

6.7 nm to 3.96 nm) with increasing reaction time and were slightly larger than the mean fibril widths of iCNF (<3 nm). By contrast CNF had a broader distribution of fibril widths that could be fit to two components with mean widths of 2.7 nm and 8.5 nm. The fibril lengths ranged from 115 nm to 165 nm for CNCs, to several hundred nm to μm for iCNFs and to several μm for CNF. Another study compared AFM measurements of height (for >1000 particles) for iCNF with low and high surface charge for bacterial CNC and wood pulp CNCs, both generated by sulfuric acid hydrolysis. The mean height for both iCNF samples was 3.3 nm but the fibril length was much shorter (0.86 μm) for the sample with the higher surface charge, compared to the low surface charge sample (3.9 μm). The bacterial and wood pulp CNCs had similar particle heights (6.7 nm, 7.0 nm) although the bacterial CNCs had a mean length of 0.52 μm compared to a value of 0.2 μm for the wood pulp CNCs.

Two studies supported by the US Nanomaterials Health Implications Research Consortium had the overall goal of understanding the variation in biological activity for CNMs with different properties.[90,102] One study was aimed at generating standard well-characterized samples for toxicological testing.[90] Two CNF samples with very similar particle diameters (64 nm, 78 nm) and lengths (6.7, 6.8 nm) were characterized along with one CNC sample with a relatively large diameter of 25.2 nm and a mean length of 267 nm. The availability of standard materials for further testing is a significant step forward for ensuring that experiments in different laboratories can be compared. In the second example the pro-inflammatory response induced by CNMs was examined for two CNFs and a series of CNCs, most of which were obtained from the Consortium.[102] Initial characterization of the samples using a combination of TEM and crystallinity measurements as well as solution DLS and zeta potential measurements was carried out. The data show variation in both length and diameter for the various CNCs and a small variation in crystallinity index. This study concluded that CNCs with mean length between 200–300 nm were more likely to cause lysosomal damage than CNFs and that the pro-inflammatory response correlated to higher crystallinity and generation of reactive

oxygen species. Although the comparison of CNFs to some CNCs showed a clear trend, a more detailed examination of measurement uncertainty would be needed to understand which of the observed variations are sufficiently large to conclude that the sample properties are different and to correlate changes in dimensional properties with biological activity.

Image analysis – progress towards automation

The papers discussed above have used a variety of different image analysis methods. In a number of cases, the microscope software is used to obtain dimensional parameters, such as length, width and height. More frequently, open source, freely available software such as Image J[103] (frequently used with EM, but also compatible with some AFM images) and Gwyddion (AFM).[104] These software packages can be used with a thresholding option to identify particles and to provide a level of automation for obtaining a wide range of dimensional parameters (minimum and maximum Feret diameters, circularity, area, perimeter, etc.). Nevertheless, both software packages are less straightforward to use with CNMs than for most inorganic nanomaterials, particularly those that are approximately spherical with a relatively narrow size distribution and can be well-dispersed on the substrate.

To date there are relatively few papers that have used automated image analysis methods for CNCs, iCNFs or CNFs. The TEM ILC used a custom ImageJ macro to automate some tasks, but still relied on manual particle selection and determination of particle width and length.[64] Some automated features in Gwyddion were employed to draw profiles through selected CNCs and then measure their length and height for the AFM ILC and in one laboratory a MATLAB routine was used to automate analysis of the extracted profiles.[50] A custom software package, Fiber App, designed for analysis of polymers, biomacromolecules and fibrils has been used to measure length and height from iCNF and CNC AFM images.[105] DNA Trace is also useful for obtaining iCNF length from AFM images and was developed for tracing the length of a variety of polymers.[106] Both Fiber App and DNA Trace have primarily been used with reasonably well-dispersed iCNFs or CNCs but may be less suitable for samples with significant agglomeration. Another software package, DiameterJ developed by NIST, can be used to rapidly measure the diameter of nanofibers from EM images, but has not yet been tested with CNMs.[107] However, it has been used to assess the width of polymer nanofibers used for tissue engineering.[108] One paper discussed above has developed custom approaches to measure dimensional parameters from AFM images. The iCNF height was measured using the scikit-image and OpenCV Python 3.6.3 libraries.[75] The iCNFs were identified by binarizing the images and applying locally adaptive thresholding. A combination of removal of noise and contamination, and a probabilistic Hough transform coupled with Canny edge detection were used to calculate the average height along the centre of each iCNF.

Two recent papers have used freely available software to assess the number of aggregates or agglomerates, as well as individual particles, for CNCs. In the Parton paper, the outlines of individual CNC were traced manually using Fiji (ImageJ) software and analyzed using the Shape Filter plug-in to obtain a range of parameters for each feature, including length, area equivalent width, perimeter, solidity, aspect ratio and rectangularity.[48] At least 250 features per sample were analyzed as a function of sonication energy. Changes in the measured parameters were used to divide the observed features into 4 groups: aggregates are disordered assemblies of crystallites, bundles are laterally connected crystallites, individual crystallites and distorted crystallites. In addition to calculating the number fraction of each class, the volume fraction was estimated by measuring the average AFM thickness (automated in Gwyddion) and assuming that the lengths measured by AFM and TEM are the same since the length vs. height and length vs. width plots are similar. This allows one to estimate volume and aspect ratios using the measured cross-sectional dimensions, rather than using either width or height.

A second recent paper from the Cranston group used Gwyddion to process AFM images and determine the height of individual particles (including any laterally aggregated CNCs that appear as a single rod-shaped feature) and aggregates (intersecting clusters of CNCs).[40] ImageJ with thresholding was then used to measure the area of individual particles and aggregates and to measure particle length along the long axis. Volumes were calculated from the area and AFM height and aspect ratios from the length (ImageJ) and height (Gwyddion). Note that in contrast to the Parton work noted above, a uniform cross sectional dimension is assumed for these estimates. Although AFM is arguably a difficult method for assessing sample dispersion, it can be used for validation of other methods as illustrated in this study.

Based on the above examples it is clear that there remains considerable scope for automated measurement of dimensional parameters from AFM or EM images of CNMs, a development that would result in a substantial decrease in the time and effort needed to obtain statistically relevant data sets. This would be particularly advantageous for TEM where the collection of a large number of images can be done reasonably quickly but the analysis is time-consuming. AFM image acquisition is still a slow step, although current developments in high-speed AFM coupled with automated analysis would be a substantial step forward. Moon and colleagues have recently developed a comprehensive image processing system, SMART (Standardized Morphology Analysis for Research and Technology) for semi-automatic analysis of both TEM and AFM images for CNCs.[109,110] The software uses a multi-step approach that includes pre-processing to enhance image quality, grouping of features to identify specific classes of CNCs (edge, isolated, aggregated) and algorithms for digital measurements of CNC dimensions (Fig. 12a and b).[110] SMART was initially tested on a subset of the images collected as part of the characterization of CNC particle size for the CNC reference material.[51] Comparison of the initial manual image analysis and SMART revealed that TEM length and width were similar for the two approaches (Fig. 12c), as were AFM
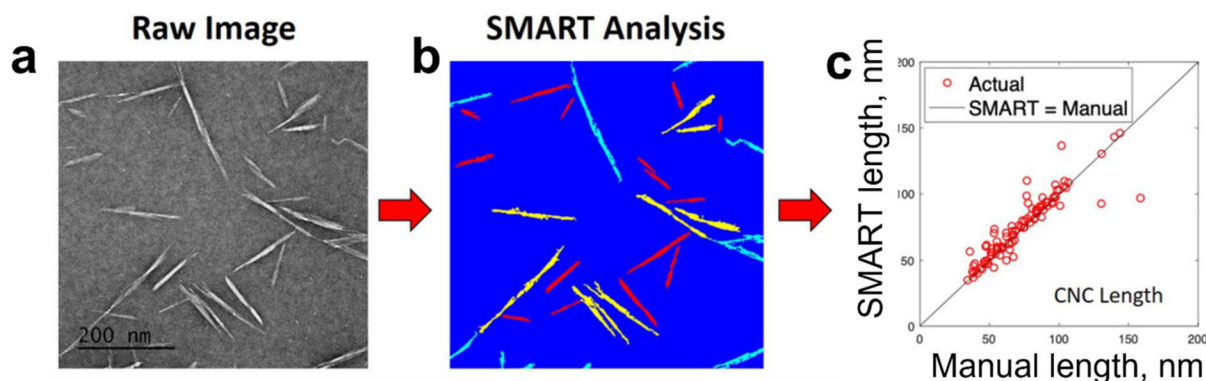
Fig. 12 Illustration of the SMART process. A TEM image before (a) and after SMART identification (b) of individual (red), agglomerated (yellow), and border (blue) CNCs. The lengths obtained by manual and SMART analysis of five images are shown in panel (c), with the solid line showing equal lengths for the two methods. This figure has been adapted from ref. 110 with permission from Springer Nature, copyright 2021.

measurements. Similar mean values and distributions were obtained for both manual and SMART analysis, despite the fact that somewhat different subsets of particles were analyzed with the two methods. This approach has the potential to significantly decrease the time required for analysis and may remove some of the analyst subjectivity in identifying individual particles.

A second paper describes the application of SMART for analysis of four image sets from a TEM ILC, again with good agreement between manual and SMART analyses.[109] This study highlights the importance of good image quality for application of SMART. It also demonstrates the utility of this approach for obtaining the area fraction of isolated CNCs, edge-touching CNCs and agglomerated CNCs, making it amenable for use for following the progress of sample dispersion. A method for rapid monitoring of size as a function of particles imaged/analyzed may in principle be useful for assessing the number of CNCs that should be analyzed for a stable dimensional measurement. Current work is directed towards extending the approaches used to the analysis of CNFs, a considerably more challenging problem, given the level of interconnectedness and branching typically observed for this material.

Conclusions and future perspectives

The papers discussed in this critical review indicate that there has been significant progress in utilizing both EM and AFM to assess dimensions of CNMs for distinguishing between sample preparation or cellulose biomass sources, as well as for obtaining fundamental mechanistic information on these materials. Although the uncertainty of the measurements is not explicitly addressed in most studies, the level of detail provided and the number of particles analyzed are now recognized to be important factors. Furthermore, the recent ILC for CNC particle size distributions as measured by AFM and TEM provides guidance on the statistics that may be needed and the uncertainty associated with these measurements. However, it

should be noted that the uncertainty due to variations related to sample preparation in different laboratories was not tested in the ILCs, and will likely increase the uncertainty. There has also been progress on using microscopy measurements for more than just size, either to assess fundamental properties of the materials (*e.g.*, chiral properties) or to measure the fractions of isolated and agglomerated particles to follow changes in dispersion of the material as a function of sonication or deposition on substrates. However, there remain studies that lack the necessary statistics and consideration of measurement uncertainty to allow one to draw meaningful conclusions on differences in CNM dimensions.

There are a number of recommendations that will help researchers address the gap in detailed studies that provide statistically relevant data sets with reported measurement uncertainty. This includes the importance of analyzing a sufficient number of particles, the requirement to analyze all individual particles in analyzed images, and the importance of considering the microscope resolution, particularly for EM. The number of particles that have to be imaged to ensure statistically meaningful data may vary with the sample, its polydispersity and its dispersion on the support used. However, one should generally aim at a minimum of 200–300 particles and monitoring dimension as a function of the number of particles analyzed is useful to identify when the size has leveled off to a constant value. There are different methods to assess uncertainty; although an inter-laboratory comparison is useful, this is far from suitable for routine experiments. Measurement of a number of independently prepared samples by different analysts in a single laboratory is a good alternative. Another method is the bottom-up approach of estimating potential uncertainties from various sources (for example, sample preparation, instrument operating conditions, *etc.*); this approach may be challenging for a non-metrology group and may lead to uncertainties that are larger than those assessed by other methods.

The progress on automation and the various approaches that have been used to assess individual isolated *vs.* agglomer-

ated particles show promise for both faster analysis and higher information content from the microscopy experiments. Although it is clear that microscopy is unlikely to be considered a routine tool for assessing sample preparation or quality control, recent studies that have correlated results from microscopy with those from complementary methods have the potential to validate the utility of more rapid methods for obtaining useful size-related information. Challenges remain in applying detailed microscopy studies to CNFs. It will be important to develop methods that are capable of not only measuring particle width but also include details on what to measure and report, and how to deal with branched, interconnected fibrils.

Finally, although dimensional measurements are important for characterizing CNMs and microscopy can be used to examine some fundamental questions about the behavior of these materials, size measurements will also be of increasing relevance for decisions as to whether a material can be classified as a nanomaterial according to the definition used by a specific regulatory body. This is a tractable problem for CNCs and iCNFs where all particles have cross-sectional dimensions that are in the nanoscale range (typically 1–100 nm). It is less obvious how one should deal with the branched structures provided by CNFs and most definitions are better suited to nanomaterials with well-defined individual particles rather than the interconnected CNF structures. Furthermore, given the complexity of the branched and interconnected structures, it is unclear that the nanosized fragment will behave in the same way as an isolated cellulose nanomaterial such as CNCs or CNFs.

Data availability

This review provides references to published literature for all data and figures. Since all data is already available in published work, there is no data associated with this review.

Conflicts of interest

There are no conflicts of interest.

Acknowledgements

References

1 D. Klemm, F. Kramer, S. Moritz, T. Lindström, M. Ankerfors, D. Gray and A. Dorris, *Angew. Chem., Int. Ed.*, 2011, **50**, 5438.

2 R. J. Moon, A. Martini, J. Nairn, J. Simonsen and J. Youngblood, *Chem. Soc. Rev.*, 2011, **40**, 3941.

3 N. Grishkewich, N. Mohammed, J. Tang and K. C. Tam, *Curr. Opin. Colloid Interface Sci.*, 2017, **29**, 32.

4 T. C. Mokhena and M. J. John, *Cellulose*, 2020, **27**, 1149.

5 A. Isogai, *J. Fiber Sci. Technol.*, 2020, **76**, 310.

6 S. Mondal, *Carbohydr. Polym.*, 2017, **163**, 301.

7 Y. Habibi, L. A. Lucia and O. J. Rojas, *Chem. Rev.*, 2010, **110**, 3479.

8 B. Frka-Petesic, T. G. Parton, C. Honorato-Rios, A. Narkevicius, K. Ballu, Q. Shen, Z. Lu, Y. Ogawa, J. S. Haataja, B. E. Droguet, R. M. Parker and S. Vignolini, *Chem. Rev.*, 2023, **123**, 12595.

9 T. Abitbol, A. Rivkin, Y. Cao, Y. Nevo, E. Abraham, T. Ben-Shalom, S. Lapidot and O. Shoseyov, *Curr. Opin. Biotechnol.*, 2016, **39**, 76.

10 ISO/TS 20477:2023, Nanotechnologies—Vocabulary for cellulose nanomaterial.

11 D. Trache, M. H. Hussin, M. K. M. Haafizc and V. K. Thakur, *Nanoscale*, 2017, **9**, 1763.

12 ISO/TS 21346:2021, Nanotechnologies—Characterization of individualized cellulose nanofibril samples.

13 A. Isogai, T. Saito and H. Fukuzumi, *Nanoscale*, 2011, **3**, 71.

14 P. A. Larsson, A. V. Riazanova, G. C. Ciftci, R. Rojas, H. H. Øvrebø, L. Wågberg and L. A. Berglund, *Cellulose*, 2019, **26**, 1565.

15 Z. J. Jakubek, M. Chen, M. Couillard, T. Leng, L. Liu, S. Zou, U. Baxa, J. D. Clogston, W. Hamad and L. J. Johnston, *J. Nanopart. Res.*, 2018, **20**, 98.

16 M. Shimizu, T. Saito, Y. Nishiyama, S. Iwamoto, H. Yano, A. Isogai and T. Endo, *Macromol. Rapid Commun.*, 2016, **37**, 1581.

17 H. Kangas, P. Lahtinen, A. Sneck, A.-M. Saariaho, O. Laitinen and E. Hellén, *Nord. Pulp Pap. Res. J.*, 2014, **29**, 129.

18 European Commission, *Commission Recommendation of 10.06.2022 on the Definition of Nanomaterial; 022/C229/01*, European Union, Brussels, 2022.

19 D. R. Boverhof, C. M. Bramante, J. H. Butala, S. F. Clancy, M. Lafranconi, J. West and S. C. Gordon, *Regul. Toxicol. Pharmacol.*, 2015, **73**, 137.

20 K. Rasmussen, J. R. Sintes and H. Rauscher, *Nat. Nanotechnol.*, 2024, **19**, 132.

21 *Chemical Substances When Manufactured or Processed as Nanoscale Materials: TSCA Reporting and Recordkeeping Requirements, OPPT-2010-0572-0137*. 2017: Environmental Protection Agency EPA, Washington.

22 *Canada Framework for the Risk Assessment of Manufactured Nanomaterials under the Canadian Environmental Protection Act, 1999. Environment and Climate Change Canada, Health Canada*. 2022.

23 E. J. Foster, R. J. Moon, U. P. Agarwal, M. J. Bortner, J. Bras, S. Camarero-Espinosa, K. J. Chan, M. J. D. Clift, E. D. Cranston, S. J. Eichhorn, D. M. Fox, W. Y. Hamad, L. Heux, B. Jean, M. Korey, W. Nieh, K. J. Ong, M. S. Reid,

S. Renneckar, R. Roberts, J. A. Shatkin, J. Simonsen, K. Stinson-Bagby, N. Wanasekaraq and J. Youngblood, *Chem. Soc. Rev.*, 2018, **47**, 2609.

24 N. Feltin, L. Crouzier, A. Delvallée, F. Pellegrino, V. Maurino, D. Bartczak, H. Goenaga-Infante, O. Taché, S. Marguet, F. Testard, S. Artous, F. Saint-Antonin, C. Salzmann, J. Deumer, C. Gollwitzer, R. Koops, N. Sebaïhi, R. Fontanges, M. Neuwirth, D. Bergmann, D. Hüser, T. Klein and V.-D. Hodoroaba, *Nanomaterials*, 2023, **313**, 993.

25 E. A. Grulke, X. Wu, Y. Ji, E. Buhr, K. Yamamoto, N. W. Song, A. B. Stefaniak, D. Schwegler-Berry, W. W. Burchett, J. Lambert and A. J. Stromberg, *Metrologia*, 2018, **55**, 254.

26 V. Kestens, G. Roebben, J. Herrmann, A. Jamting, V. Coleman, C. Minelli, C. Clifford, P.-J. De Temmerman, J. Mast, L. Junjie, F. Babick, H. Cölfen and H. Emons, *J. Nanopart. Res.*, 2016, **18**, 171.

27 ISO/TR 19716:2016, Nanotechnologies – Characterization of cellulose nanocrystals.

28 S. Elazzouzi-Hafraoui, Y. Nishiyama, J.-L. Putaux, L. Heux, F. Dubreuil and C. Rochas, *Biomacromolecules*, 2009, **9**, 57.

29 I. Usov, G. Nyström, J. Adamcik, S. Handschin, C. Schütz, A. Fall, L. Bergström and R. Mezzenga, *Nat. Commun.*, 2015, **6**, 7564.

30 Y. Nishiyama, *J. Wood Sci.*, 2009, **55**, 241.

31 L. Brinchi, F. Cotana, E. Fortunati and J. M. Kenney, *Carbohydr. Polym.*, 2013, **94**, 154.

32 W. Y. Hamad and T. Q. Hu, *Can. J. Chem. Eng.*, 2010, **88**, 392.

33 S. Beck, J. Bouchard and R. Berry, *Biomacromolecules*, 2012, **13**, 1486–1494.

34 A. Brinkmann, M. Chen, M. Couillard, Z. Jakubek, T. Leng and L. J. Johnston, *Langmuir*, 2016, 6105.

35 B. Zakani and D. Grecov, *Carbohydr. Polym.*, 2022, **291**, 119651.

36 ISO/TS 23151:2021, Nanotechnologies—Particle size distribution for cellulose nanocrystals.

37 M. E. Girard, D. Vidal, F. Bertrand, J. R. Tavares and M.-C. Heuzey, *Ultrason. Sonochem.*, 2021, **71**, 105378.

38 C. Campano, P. Lopez-Exposito, L. Gonzalez-Aguilera, A. Blanco and C. Negro, *Carbohydr. Polym.*, 2021, **254**, 117271.

39 A. Mukherjee and V. A. Hackley, *Analyst*, 2018, **143**, 4731.

40 M. A. Johns, C. Lam, B. Zakani, L. Melo, E. R. Grant and E. D. Cranston, *Cellulose*, 2023, **30**, 8259.

41 O. M. Vanderfleet, J. Winitsky, J. Bras, J. Godoy-Vargas, V. Lafitte and E. D. Cranston, *Cellulose*, 2021, **28**, 10239.

42 F. Cherhal, F. Cousin and I. Capron, *Langmuir*, 2015, **31**, 5596.

43 M. Uhlig, A. Fall, S. Wellert, M. Lehmann, S. Prevost, L. Wagberg, R. V. Klitzing and G. Nyström, *Langmuir*, 2016, **32**, 442.

44 M. Chen, J. Parot, V. A. Hackley, S. Zou and L. J. Johnston, *Cellulose*, 2021, **28**, 1933.

45 M. T. Postek, A. Vladár, J. Dagata, N. Farkas, B. Ming, R. Wagner, A. Raman, R. J. Moon, R. Sabo, T. H. Wegner and J. Beecher, *Meas. Sci. Technol.*, 2011, **22**, 024005.

46 R. R. Lahiji, X. Xu, R. Reifenberger, A. Raman, A. Rudie and R. J. Moon, *Langmuir*, 2010, **26**, 4480.

47 G. Sèbe, F. Ham-Pichavant, E. Ibarboure, A. L. C. Koffi and P. Tingaut, *Biomacromolecules*, 2012, **13**, 570.

48 T. G. Parton, R. M. Parker, G. T. Van De Kerkhof, A. Narkevicius, J. S. Haataja, B. Frka-Petesic and S. Vignolini, *Nat. Commun.*, 2022, **13**, 2657.

49 VAMAS, available from: https://www.vamas.org/twa34/index.html (accessed May 28, 2024).

50 M. Bushell, J. Meija, M. Chen, W. Batchelor, C. Browne, J.-Y. Cho, C. A. Clifford, Z. Al-Rekabi, O. Vanderfleet, E. Cranston, M. Lawn, V. A. Coleman, G. Nyström, M. Arcari, R. Mezzenga, B. C. Park, L. Ren, T. Saito, Y. Kaku, R. Wagner and L. J. Johnston, *Cellulose*, 2021, **28**, 1387.

51 NRC Certified reference material, http://www.nrc.ca/crm, (accessed May 28, 2024).

52 G. Delepierre, O. M. Vanderfleet, E. Niinivaara, B. Zakani and E. D. Cranston, *Langmuir*, 2021, **37**, 8393.

53 M. S. Reid, M. Villalobos and E. D. Cranston, *Langmuir*, 2017, **33**, 1583.

54 C. Schütz, J. V. Rie, S. Eyley, A. Gencer, H. V. Gorp, S. Rosenfeldt, K. Kang and W. Thielemans, *ACS Sustainable Chem. Eng.*, 2018, **6**, 8317.

55 M. Nordenström, A. Fall, G. Nyström and L. Wagberg, *Langmuir*, 2017, **33**, 9772.

56 S. L. Leong, S. I. X. Tiong, S. P. Siva, F. Ahamed, C.-H. Chan, C. L. Lee, I. M. L. Chew and Y. K. Ho, *J. Environ. Chem. Eng.*, 2022, **10**, 108145.

57 K. S. Salem, N. K. Kasera, M. A. Rahman, H. Jameel, Y. Habibi, S. J. Eichhorn, A. D. French, L. Pal and L. A. Lucia, *Chem. Soc. Rev.*, 2023, **52**, 6417.

58 V. Grachev, O. Deschaume, P. R. Lang, M. P. Lettinga, C. Bartic and W. Thielemans, *Nanomaterials*, 2024, **14**, 455.

59 M. Kaushik, C. Fraschini, G. Chauve, J.-L. Putaux and A. Moores, in *The Transmission Electron Microscope - Theory and Application*, ed, K. Maaz, IntechOpen, 2015, DOI: 10.5772/60985.

60 K. L. Stinson-Bagby, R. Roberts and E. J. Foster, *Carbohydr. Polym.*, 2018, **186**, 429.

61 Y. Ogawa and J.-L. Putaux, *Cellulose*, 2019, **26**, 17.

62 L. C. E. D. Silva, A. Cassago, L. C. Battirola, M. D. C. Gonçalves and R. V. Portugal, *Cellulose*, 2020, **27**, 5435.

63 C. Campano, A. Balea, A. N. Blanco and C. Negro, *Cellulose*, 2020, **27**, 4871.

64 J. Meija, M. Bushell, M. Couillard, S. Beck, J. Bonevich, K. Cui, J. Foster, J. Will, D. Fox, W. Cho, M. Heidelmann, B. C. Park, Y. C. Park, L. Ren, L. Xu, A. Stefaniak, A. K. Knepp, R. Theissmann, H. Purwin, Z. Wang, N. de Val and L. J. Johnston, *Anal. Chem.*, 2020, **92**, 13434.

65 L. Chen, Q. Wang, K. Hirth, C. Baez, U. P. Agarwal and J. Y. Zhu, *Cellulose*, 2015, **22**, 1753.

66 C. Browne, V. S. Raghuwanshi, M. Lin, G. Garnier and W. Batchelor, *Colloids Surf., A*, 2022, **651**, 129532.

67 B. S. L. Brito, F. V. Pereira, J.-L. Putaux and B. Jean, *Cellulose*, 2012, **19**, 1527.

68 F. Cherhal, F. Cousin and I. Capron, *Langmuir*, 2015, **31**, 5596.

69 M. Uhlig, A. Fall, S. Wellert, M. Lehmann, S. Prevost, L. Wagberg, R. V. Klitzing and G. Nyström, *Langmuir*, 2015, **32**, 442.

70 M. Chen, J. Parot, A. Mukherjee, M. Couillard, S. Zou, V. A. Hackley and L. J. Johnston, *Cellulose*, 2020, **27**, 2015.

71 X. Guan, R. Cueto, P. Russo, Y. Qi and Q. Wu, *Biomacromolecules*, 2012, **13**, 2671.

72 C. Ruiz-Palomero, M. L. Soriano and M. Valcárcel, *Microchim. Acta*, 2017, **184**, 1069.

73 T. Saito, M. Hirota, N. Tamura, S. Kimura, H. Fukuzumi, L. Heux and A. Isogai, *Biomacromolecules*, 2009, **10**, 1992.

74 S. Iwamoto, W. Kai, A. Isogai and T. Iwata, *Biomacromolecules*, 2009, **10**, 2571.

75 T. Willhammar, K. Daicho, D. N. Johnstone, K. Kobayashi, Y. Liu, P. A. Midgley, L. Bergström and T. Saito, *ACS Nano*, 2021, **15**, 2730.

76 K. Daicho, T. Saito, S. Fujisawa and A. Isogai, *ACS Appl. NanoMater.*, 2018, **1**, 5774.

77 L. Geng, N. Mittal, C. Zhan, F. Ansari, P. R. Sharma, X. Peng, B. S. Hsiao and L. D. SöDerberg, *Macromolecules*, 2018, **15**, 1498.

78 A. J. Benítez, F. Lossada, B. Zhu, T. Rudolph and A. Walther, *Biomacromolecules*, 2016, **17**, 2417.

79 M. Arcari, E. Zuccarella, R. Axelrod, J. Adamcik, A. Sánchez-Ferrer, R. Mezzenga and G. Nyström, *Biomacromolecules*, 2019, **20**, 1288.

80 G. Nyström, M. Arcari, J. Adamcik, I. Usov and R. Mezzenga, *ACS Nano*, 2018, **12**, 5141.

81 R. Shinoda, T. Saito, Y. Okita and A. Isogai, *Biomacromolecules*, 2012, **13**, 842.

82 L. V. Hai, H. C. Kim, A. Kafy, L. Zhai, J. W. Kim and J. Kim, *Cellulose*, 2017, **24**, 3301.

83 A. N. Fernandes, L. H. Thomas, C. M. Altaner, P. Callow, V. T. Forsyth, D. C. Apperley, C. J. Kennedy and M. C. Jarvis, *Proc. Natl. Acad. Sci. U. S. A.*, 2011, **108**, E1195.

84 Y. Ogawa, *Nanoscale*, 2019, **11**, 21767.

85 R. J. Moon, C. L. Hensdal, S. Beck, A. Fall, J. Costa, E. Kojima, T. Abitbol, V. Raghuwanshi, C. Walker and W. Batchelor, *Tappi J.*, 2023, **22**, 116.

86 S. Ang, J. R. Narayanan, W. Kargupta, V. Haritos and W. Batchelor, *Cellulose*, 2020, **27**, 4189.

87 B. D. Mattos, B. L. Tardy and O. J. Rojas, *Biomacromolecules*, 2019, **20**, 2657.

88 M. S. Toivonen, O. D. Onelli, G. Jacucci, V. Lovikka, O. J. Rojas, O. Ikkala and S. Vignolini, *Adv. Mater.*, 2018, **30**, 1704050.

89 D. Bitounis, G. Pyrgiotakis, D. Bousfield and P. Demokritou, *NanoImpact*, 2019, **15**, 100171.

90 G. Pyrgiotakis, W. Luu, Z. Zhang, N. Vaze, G. Deloid, L. Rubio, W. a. C. Graham, D. C. Bell, D. Bousfield and P. Demokritou, *Cellulose*, 2018, **25**, 2303.

91 L. Zhai, H. C. Kim, J. W. Kim and J. Kim, *Sci. Rep.*, 2020, **10**, 11744.

92 U. Ringania, J. Harrison, R. J. Moon and M. S. Bhamla, *Cellulose*, 2022, **29**, 5575.

93 Q. Q. Wang, J. Y. Zhu, R. Gleisner, T. A. Kuster, U. Baxa and S. E. McNeil, *Cellulose*, 2012, **19**, 1631.

94 S. Ang, V. Haritos and W. Batchelor, *Cellulose*, 2019, **26**, 4767.

95 H. E. Cainglet, J. Tanner, N. Nasiri, C. Browne, G. Garnier and W. Batchelor, *Cellulose*, 2023, **30**, 4971.

96 S. Ahola, J. Salmi, L.-S. Johansson, J. Laine and M. Österberg, *Biomacromolecules*, 2008, **9**, 1273.

97 L. Shi, L. Kang, J. Gong, X. Zhang, J. Liao, L. Mo and J. Li, *Ind. Crops Prod.*, 2022, **180**, 114742.

98 L. Berglund, M. Noël, Y. Aitomäki, T. Öman and K. Oksman, *Ind. Crops Prod.*, 2016, **92**, 84.

99 S. Tagawa, K. Ishida, T. Tsuji and T. Kondo, *Cellulose*, 2021, **28**, 2917.

100 X. Jiang, J. B. Mietner and J. R. G. Navarro, *Cellulose*, 2023, **30**, 2929.

101 F. Jiang and Y.-L. Hsieh, *Carbohydr. Polym.*, 2013, **95**, 32.

102 X. Wang, C. H. Chang, J. Jiang, Q. Liu, Y.-P. Liao, J. Lu, L. Li, X. Liu, J. Kim, A. Ahmed, A. E. Nel and T. Xia, *Small*, 2019, **15**, 1901642.

103 ImageJ. Available from: **https://imagej.net/ij/index.html** (accessed May 25, 2024).

104 Gwyddion, Available from: **https://gwyddion.net/**(accessed May 25, 2024).

105 I. Usov and R. Mezzenga, *Macromolecules*, 2015, **48**, 1269.

106 A. Mikhaylov, S. K. Sekatskii and G. Dietler, *J. Adv. Microsc. Res.*, 2013, **8**, 241.

107 N. A. Hotaling, K. Bharti, H. Kriel and C. G. Simon Jr., *Biomaterials*, 2015, **61**, 327.

108 S. Kyriakou, S. Acosta, I. E. Maachi, S. Rütten and S. Jockenhoevel, *Polymers*, 2023, **15**, 4332.

109 S. Yucel, R. J. Moon, L. J. Johnston, D. M. Fox, B. C. Park, E. J. Foster and S. R. Kalidindi, *Cellulose*, 2022, **29**, 9035.

110 S. Yucel, R. J. Moon, L. J. Johnston, B. Yucel and S. R. Kalidindi, *Cellulose*, 2021, **28**, 2183.